Science Advances
AAAS

Supplementary Materials for

Glyoxal fixation: An approach to solve immunohistochemical problem in neuroscience research

Kohtarou Konno *et al.*

Corresponding author: Masahiko Watanabe, watamasa@med.hokudai.ac.jp

Sci. Adv. **9**, eadf7084 (2023)
DOI: 10.1126/sciadv.adf7084

This PDF file includes:

In all supplemental figures, bars on each column represent SEM. ****, $p < 0.0001$; ***, $p < 0.0001$; **, $p < 0.001$; *, $p < 0.05$; n.s., statistically not significant. unpaired *t*-test or one-way ANOVA with post hoc Tukey test. For detailed statistics, see Table S2. *Abbreviations*. Cb, cerebellum; Cx, cortex; DG, dentate gyrus; GL, granular layer; Hi, hippocampus; Mb, midbrain; ML, molecular layer; MO, medulla oblongata; OB, olfactory bulb; PCL, Purkinje cell layer; Py, pyramidal cell layer; Ra, stratum radiatum; St, striatum; Th, thalamus; I~VI, cortical layer I through VI.

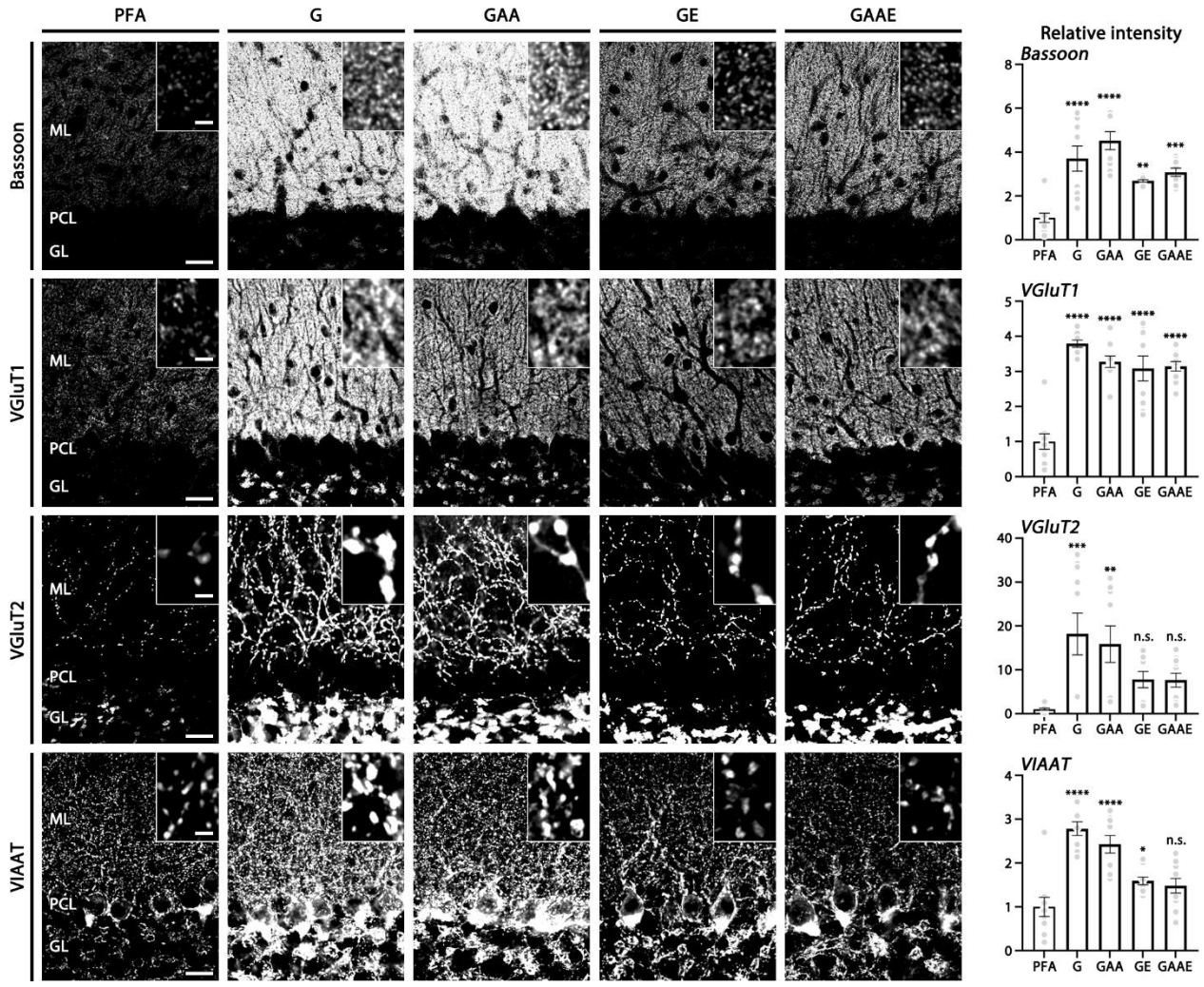

Fig. S1. Intensified immunofluorescence signals for presynaptic molecules in glyoxal-fixed cerebellar cortex. Immunofluorescence for Bassoon, vesicular glutamate transporters VGluT1 and VGluT2, and vesicular inhibitory amino acid transporter VIAAT in tissues fixed by 4% PFA or glyoxal with different composition: 3% glyoxal (G), 3% glyoxal/0.8% acetic acid (GAA), 3% glyoxal/20% EtOH (GE), and 3% glyoxal/0.8% acetic acid/20% ethanol (GAAE). Insets indicate magnified punctate images in the molecular layer. Histograms showing the mean relative fluorescent intensity in each glyoxal fixative normalized to that in 4% PFA. Each data was calculated from 10 images per mouse (n = 2 mice). Scale bars, 20 μm; insets, 2 μm.

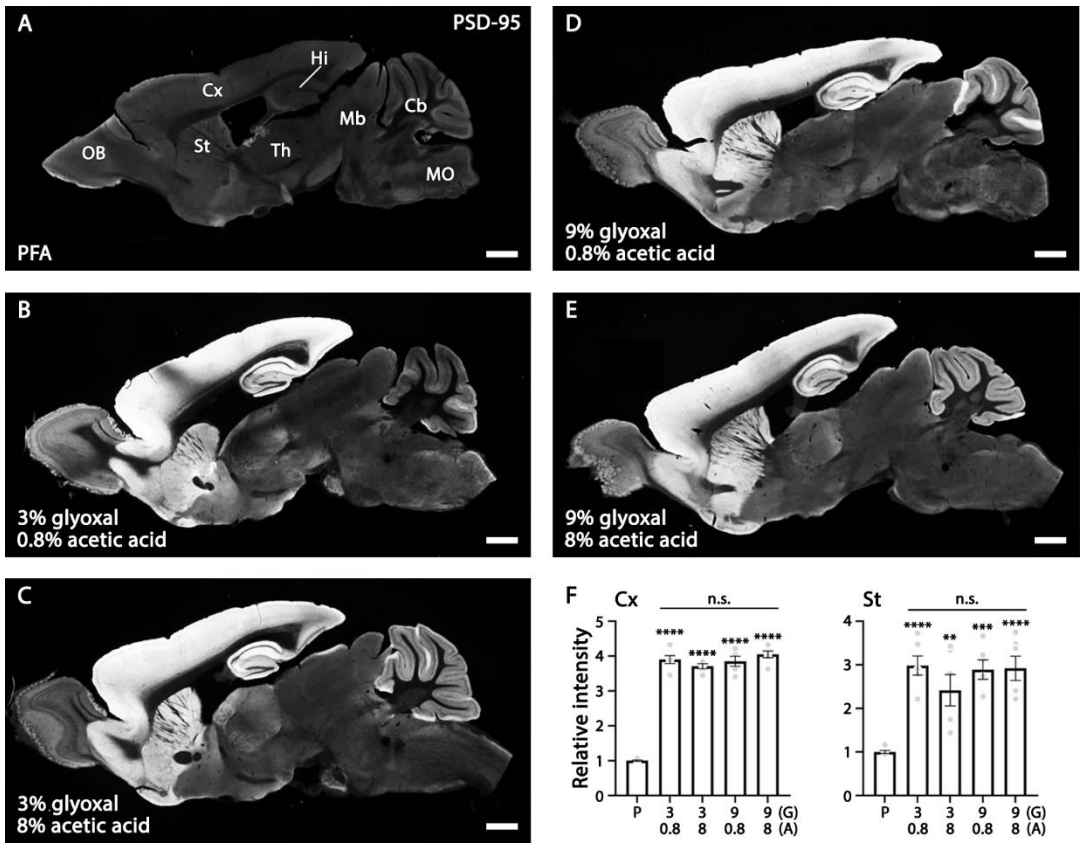

Fig. S2. Effect of glyoxal/acetic acid (GAA) fixative with different concentrations on PSD-95 immunofluorescence in parasagittal brain sections. (**A** to **E**) 4% PFA (**A**), 3% glyoxal (G)/0.8% acetic acid (A) (**B**), 3% glyoxal/8% acetic acid (**C**), 9% glyoxal/0.8% acetic acid (**D**), and 9% glyoxal/8% acetic acid (**E**). (**F**) Histograms showing the mean relative fluorescent intensity in respective glyoxal fixatives in the somatosensory cortex (left) and striatum (right) normalized to that in 4% PFA. Each data was calculated from 3 images per mouse (n = 2 mice). Significant intensification is noted between 4% PFA and each of four GAA fixatives with different concentrations, but not among four glyoxal fixatives. Scale bars, 1 mm.

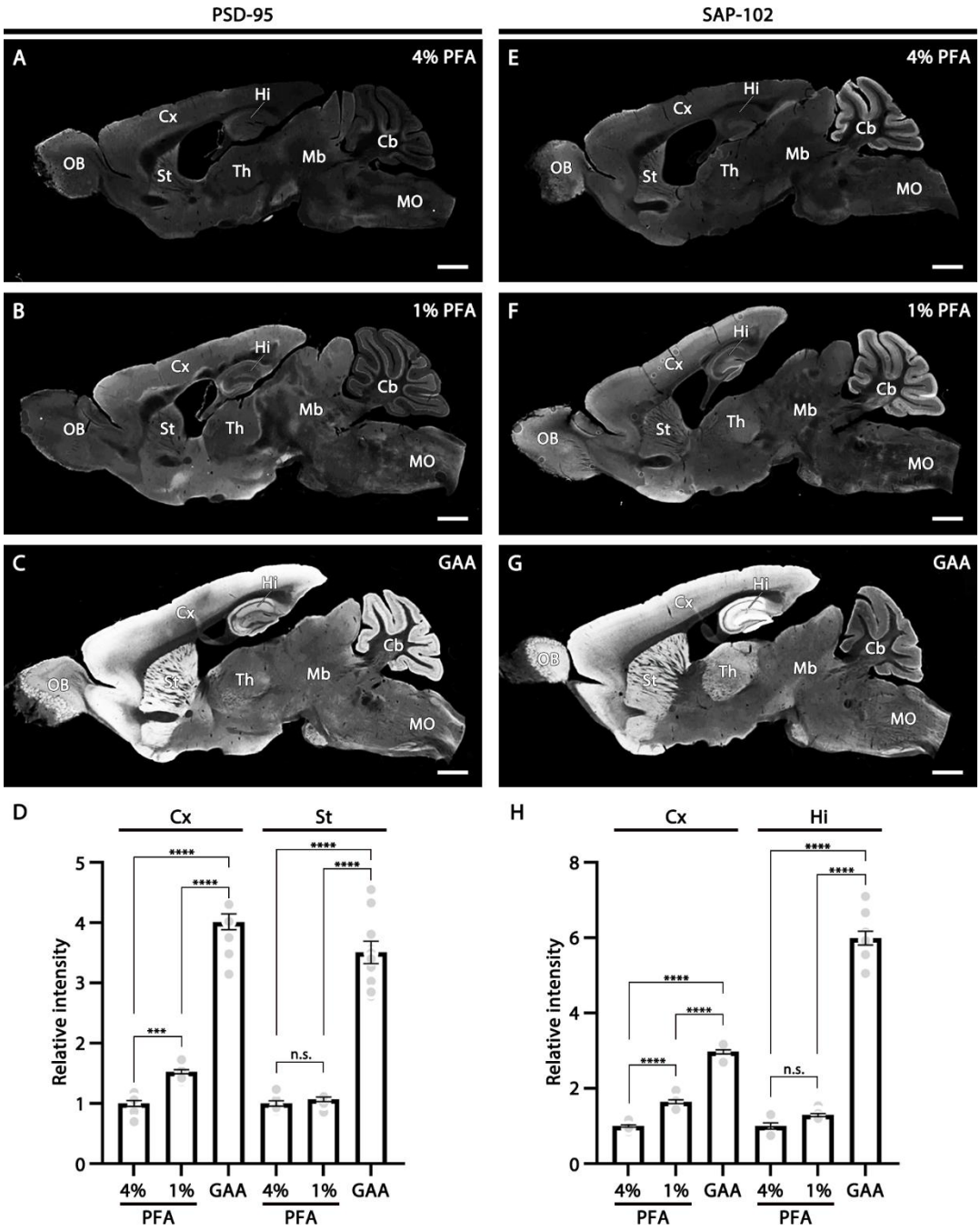

Fig. S3. 9% glyoxal/8% acetic acid (GAA) is superior to low concentration (1%) PFA in immunofluorescence for excitatory postsynaptic scaffolding proteins. (**A** to **C**) Immunofluorescence for PSD-95 in parasagittal brain sections fixed by 4% PFA (**A**), 1% PFA (**B**), and GAA (**C**). (**E** to **G**) Immunofluorescence for SAP-102 in parasagittal brain sections fixed by 4% PFA (**E**), 1% PFA (**F**), and GAA (**G**). (**D** and **H**) Histograms showing the mean relative intensity for PSD-95 (**D**) and SAP-102 (**H**) in the somatosensory cortex (Cx), striatum (St), and

hippocampus (Hi). The intensity in 1% PFA- and GAA-fixed sections are normalized to that in 4% PFA-fixed sections. Each data was calculated from 5 images per mouse (n = 2 mice). Scale bars, 1 mm.

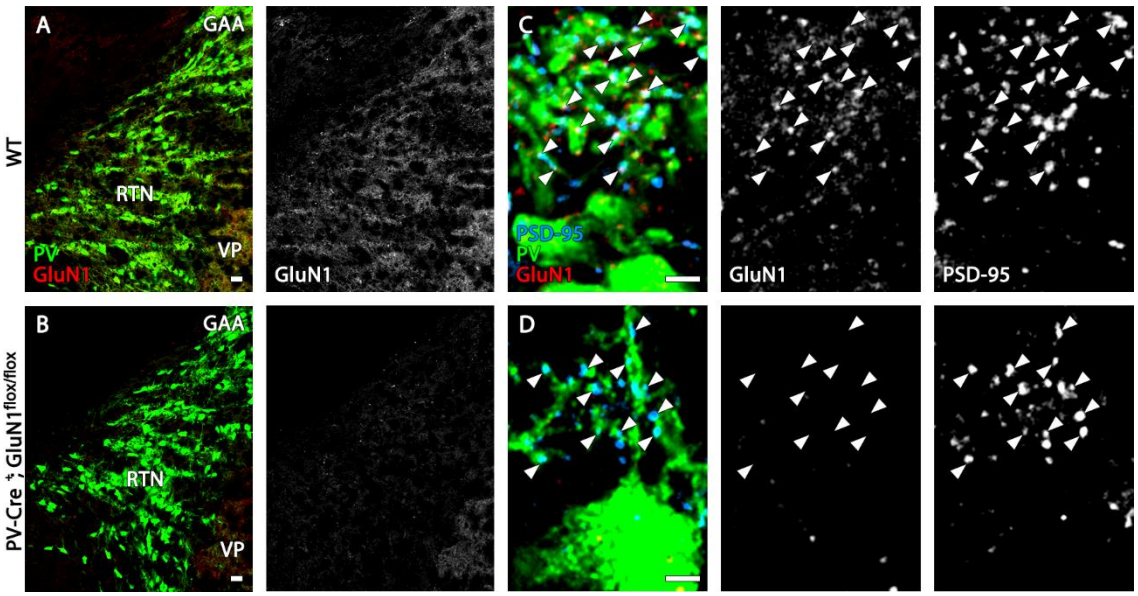

Fig. S4. The specificity of GluN1 immunohistochemistry in GAA-fixed brains. Immunofluorescence for parvalbumin (PV) and GluN1 (**A**, **B**) and for PV, GluN1, and PSD-95 (**C**, **D**) in the reticular thalamic nucleus (RTN) of wild-type (**A**, **C**) and PV-Cre^{+}; GluN1$^{flox/flox}$ (**B**, **D**) mouse brains. In wild-type RTN, GluN1 is detected as punctate labeling on PV(+) dendrites and overlapped with PSD-95 (arrowheads). The absence of GluN1 immunostaining on PSD-95(+) synapses on PV(+) dendrites in PV-Cre^{+}; GluN1$^{flox/flox}$ mouse verifies the specificity of GluN1 labeling in GAA-fixed sections. Arrowheads indicate PSD-95(+) excitatory synapses on PV(+) dendrites. RTN, reticular thalamic nucleus; VP, ventral posterior nucleus of the thalamus. Scale bars, **A** and **B**, 20 μm; **C** and **D**, 2 μm.

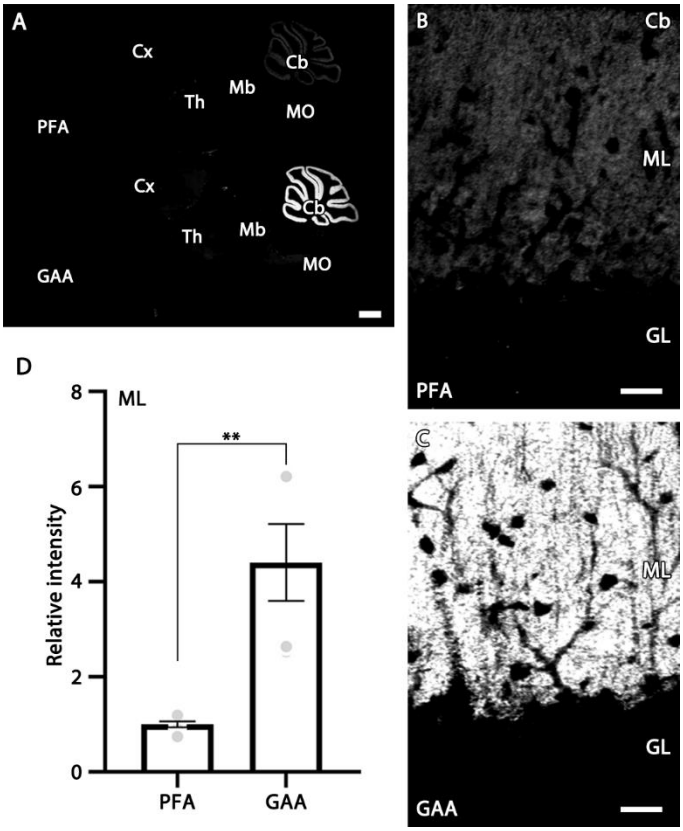

Fig. S5. Glyoxal fixation improves immunofluorescence using paraffin sections. (**A**) Immunofluorescence for GluD2 in parasagittal brain sections. Brains fixed by 4% PFA (upper) and 9% glyoxal/8% acetic acid (GAA, lower) were embedded in the same paraffin block. Both sections were mounted on the same glass slide and incubated in the same drops of antibody solution. (**B** and **C**) Magnified images of the cerebellar cortex (**B**, PFA; **C**, GAA) taken from **A**. (**D**) Histogram showing the mean relative intensity of GluD2 signals in the cerebellar molecular layer. The relative intensity in GAA fixation was normalized to that in PFA fixation. Each data was calculated from 3 images per mouse (n = 2 mice). Scale bars, **A**, 1 mm; **B** and **C**, 20 μm.

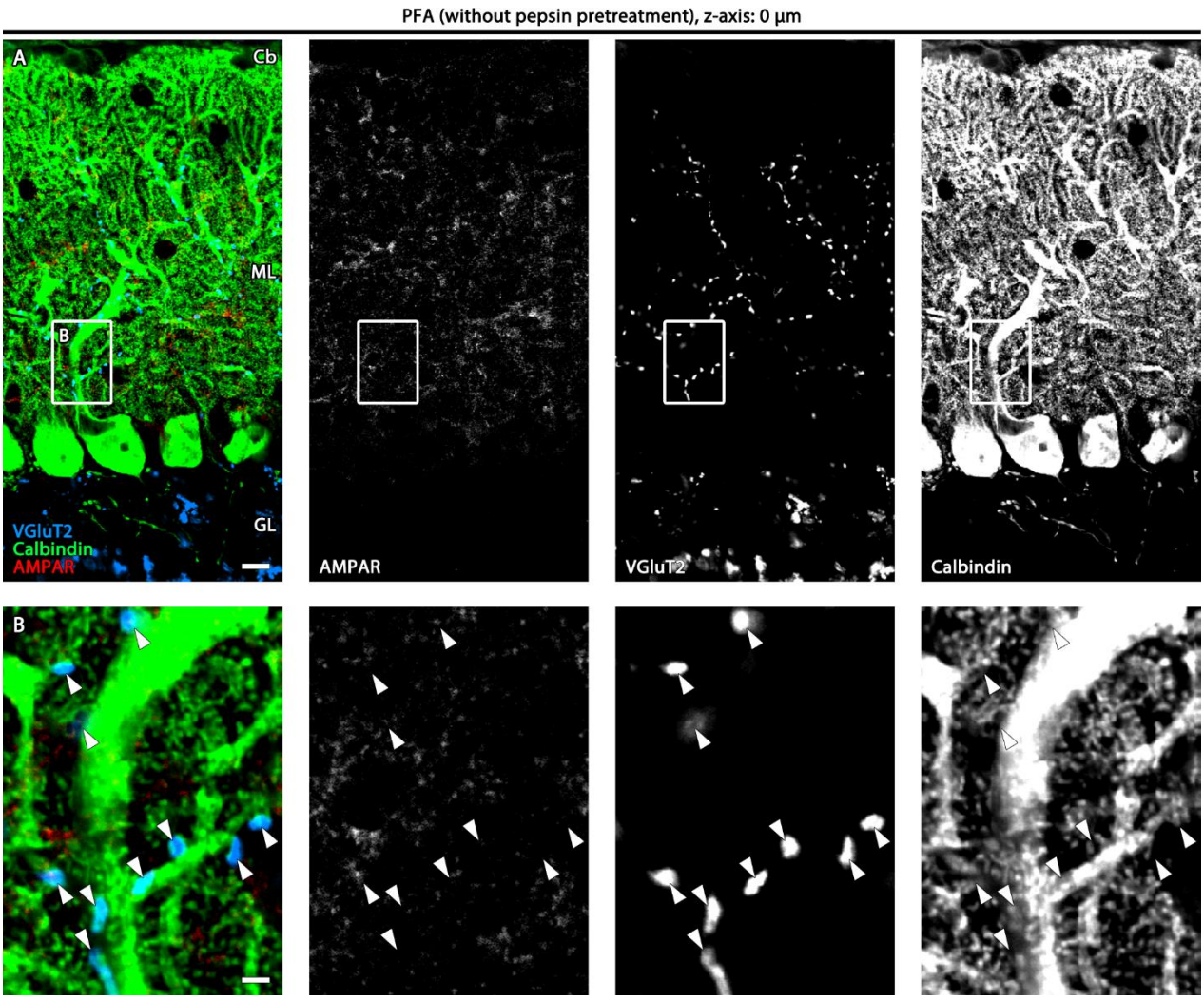

Fig. S6. Detection of glial, but not synaptic, AMPAR in PFA-fixed pepsin-untreated sections. Triple immunofluorescence for AMPAR (red; pan-AMPAR antibody), VGluT2 (blue), and calbindin (green) in the cerebellar cortex. A boxed region in **A** is magnified in **B**. Arrowheads indicate VGluT2(+) climbing fiber terminals in contact with Purkinje cell dendrites. Note weak AMPAR labeling is detected in calbindin(-) neuropil, but not at climbing fiber-Purkinje cell synapses, suggesting detection of glial, not synaptic, AMPA in PFA-fixed pepsin-untreated sections. Scale bars, **A**, 10 µm; **B**, 2 µm.

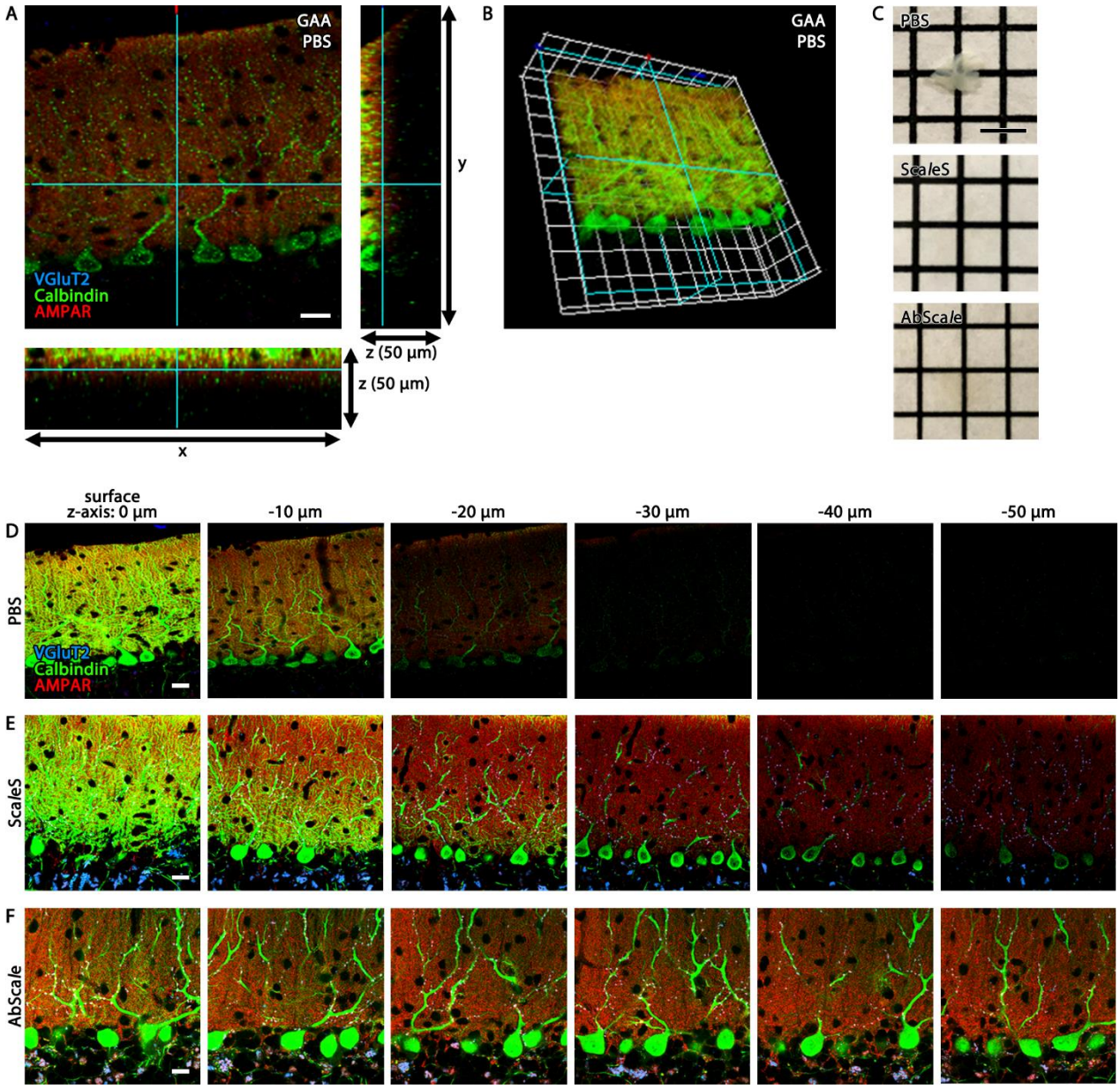

Fig. S7. Deep z-axis imaging for AMPAR as well as for VGluT2 and calbindin. Immunofluorescence for AMPAR (red), VGluT2 (blue), and calbindin (green) was applied to GAA-fixed 100 μm-thick cerebellar sections (**A**, **B**, **D** to **F**). (**A** and **B**) The *xy*, *xz*, and *yz* planes of images (**A**) and 3D images (**B**), which were untreated with tissue clearing methods and reconstructed from consecutive images along the z-axis (1.0 μm step). (**C**) GAA-fixed 100 μm-thick cerebellar sections without (upper, PBS) or with treatment of the tissue clearing by Sca*l*eS (middle) or AbSca*l*e (lower). (**D** to **F**) Consecutive triple immunofluorescence images in GAA-fixed cerebellar sections treated without (**D**) or with Sca*l*eS after immunoreaction (**E**) or AbSca*l*e during immunoreaction (**F**). Consecutive images were captured along the *z*-axis by 1 μm step, and

images at 0, 10, -20, -30, -40, and -50 μm deep from the surface are shown in this panel. Scale bars, **C**, 3 mm; **A**, **D** to **F**, 20 μm.

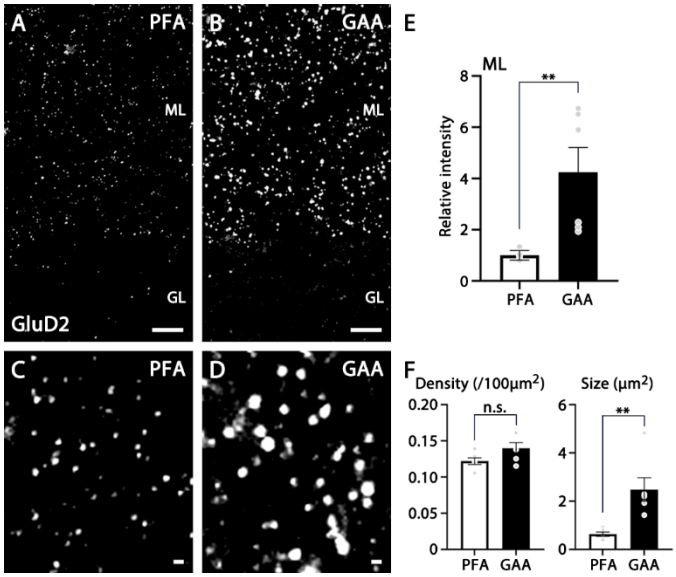

Fig. S8. GAA fixation increases the intensity of individual signals, as assessed by post-embedding immunofluorescence for GluD2 in the cerebellar cortex. (**A** to **D**) Immunofluorescence for GluD2 in Lowicryl-embedded ultrathin sections fixed by PFA (**A** and **B**) or GAA (**C** and **D**). (**E**) Histogram showing significant increase in the mean relative intensity of GluD2 in the cerebellar molecular layer by GAA fixation normalized to PFA fixation. Each value was calculated from 3 images per mouse (n = 2 mice). (**F**) Histograms showing that the size (right), but not density (left), of fluorescent signals is significantly increased by GAA fixation, as compared to PFA fixation. Each value was calculated from 3 images per mouse (n = 2 mice). Scale bars, **A** and **B**, 10 μm, **C** and **D**, 1 μm.

Fig. S9–S18. Comparisons of immunofluorescence detection for various categories of molecules in brain sections fixed by PFA (upper) and GAA (lower). For each molecule, left panels show overall staining patterns in parasagittal brain sections, while right panels show magnified images from representative regions of the brain. The mean relative intensity in PFA- and GAA-fixed representative regions was measured and normalized to that of PFA fixation, as indicated in individual Supplemental Figures. Each data was average of 5 images per mouse (n = 2 mice) and the total measured area is 0.14 mm^2, unless otherwise noted. Scale bars, low-magnification left panels, 1 mm, high-magnification right panels, 2, 10, or 50 μm (indicated in each Figure).

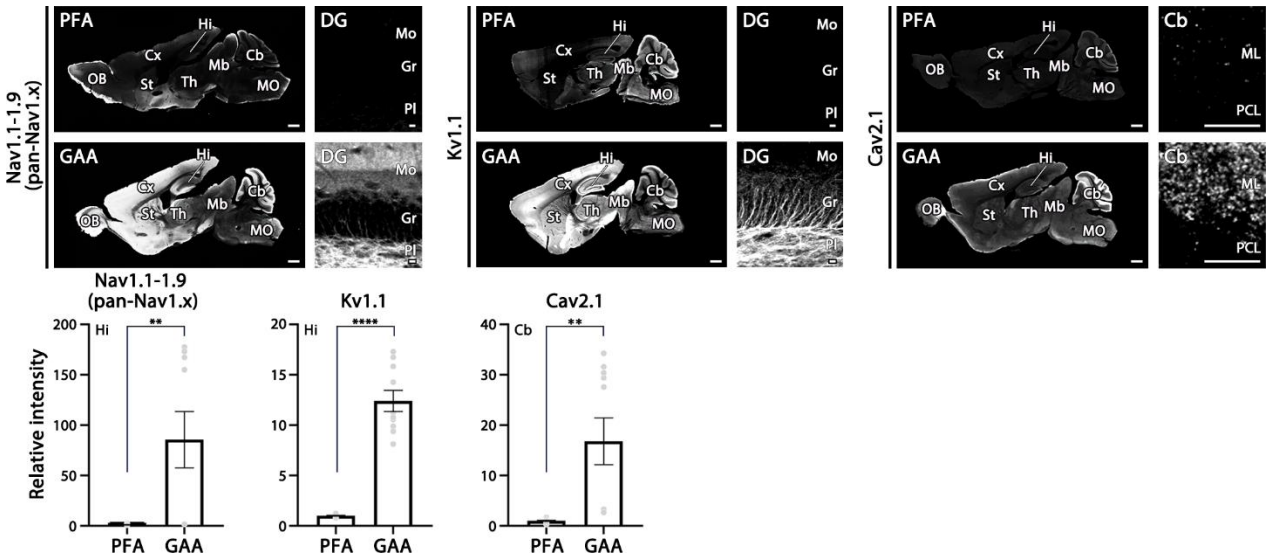

Fig. S9. Voltage-gated ion channels. The mean relative intensity is significantly increased by GAA fixation for Nav1.1-1.9 in the hippocampal dentate gyrus, Kv1.1 in the hippocampal dentate gyrus, and Cav2.1 in the cerebellum. Scale bars for high-magnification right panels, 10 μm.

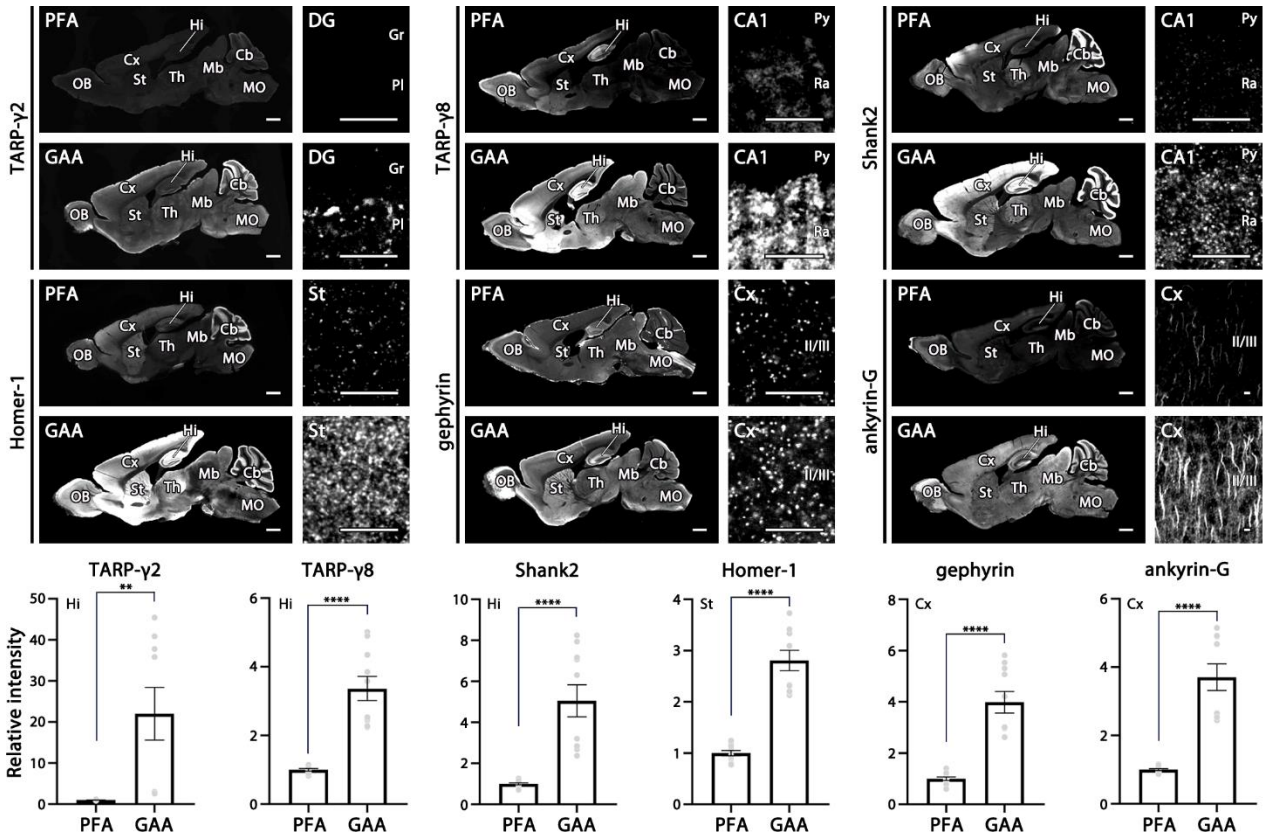

Fig. S10. Ion channel/receptor-associated molecules. The mean relative intensity is significantly increased by GAA fixation for transmembrane AMPA receptor regulatory protein-γ2 (TARP-γ2) in the hippocampal dentate gyrus, TARP-γ8 in the hippocampal CA1, Shank2 in the hippocampal CA1, Homer-1 in the striatum, gephyrin in the cortex, and ankyrin-G in the cortex. Scale bars for high-magnification right panels, 10 μm.

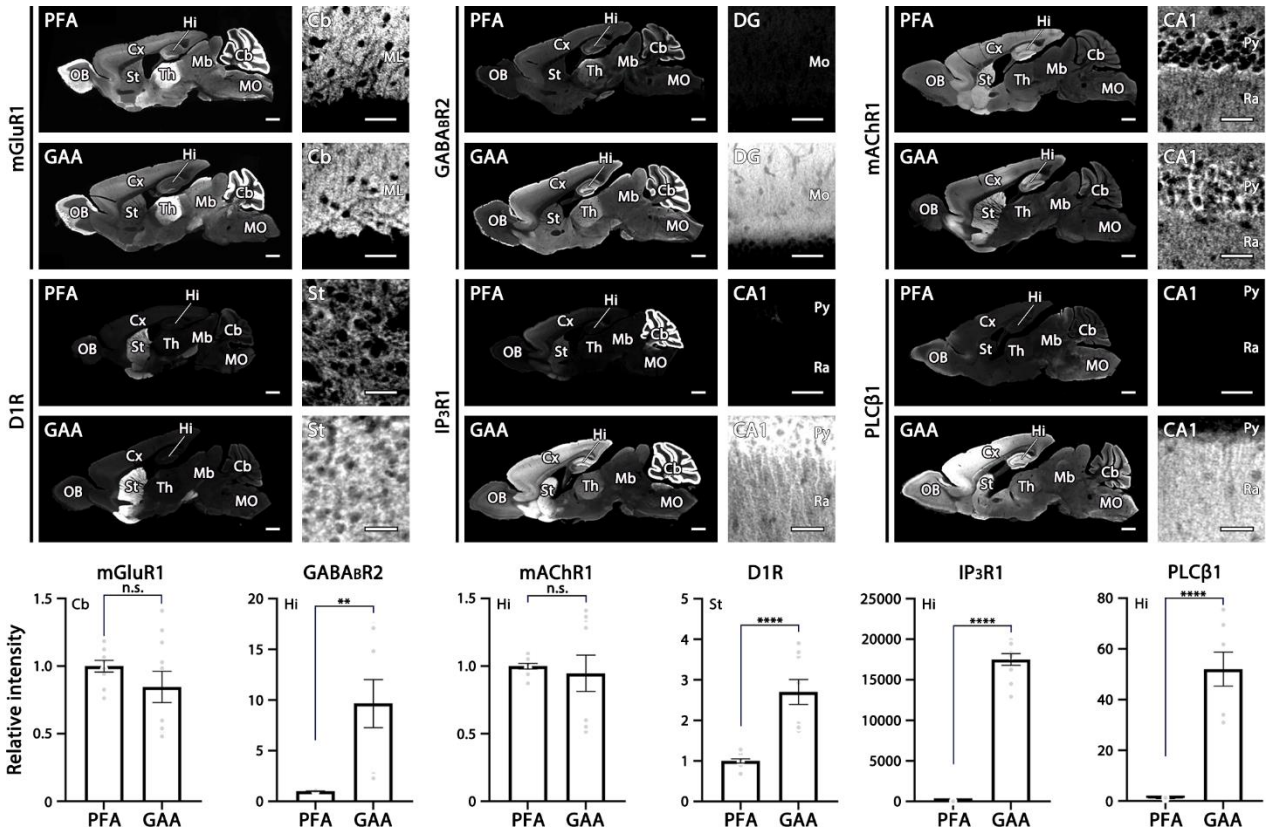

Fig. S11. Metabotropic receptors and related signaling molecules. The mean relative intensity is significantly increased by GAA fixation for $GABA_BR2$ in the hippocampal dentate gyrus, dopamine receptor D1R in the striatum, inositol triphosphate receptor IP_3R1 in the hippocampal CA1, and phospholipase PLCβ1 in the hippocampal CA1. No significant differences are noted for metabotropic glutamate receptor mGluR1 in the cerebellum and muscarinic acetylcholine receptor mAChR1 in the hippocampal CA1. Scale bars for high-magnification right panels, 50 μm.

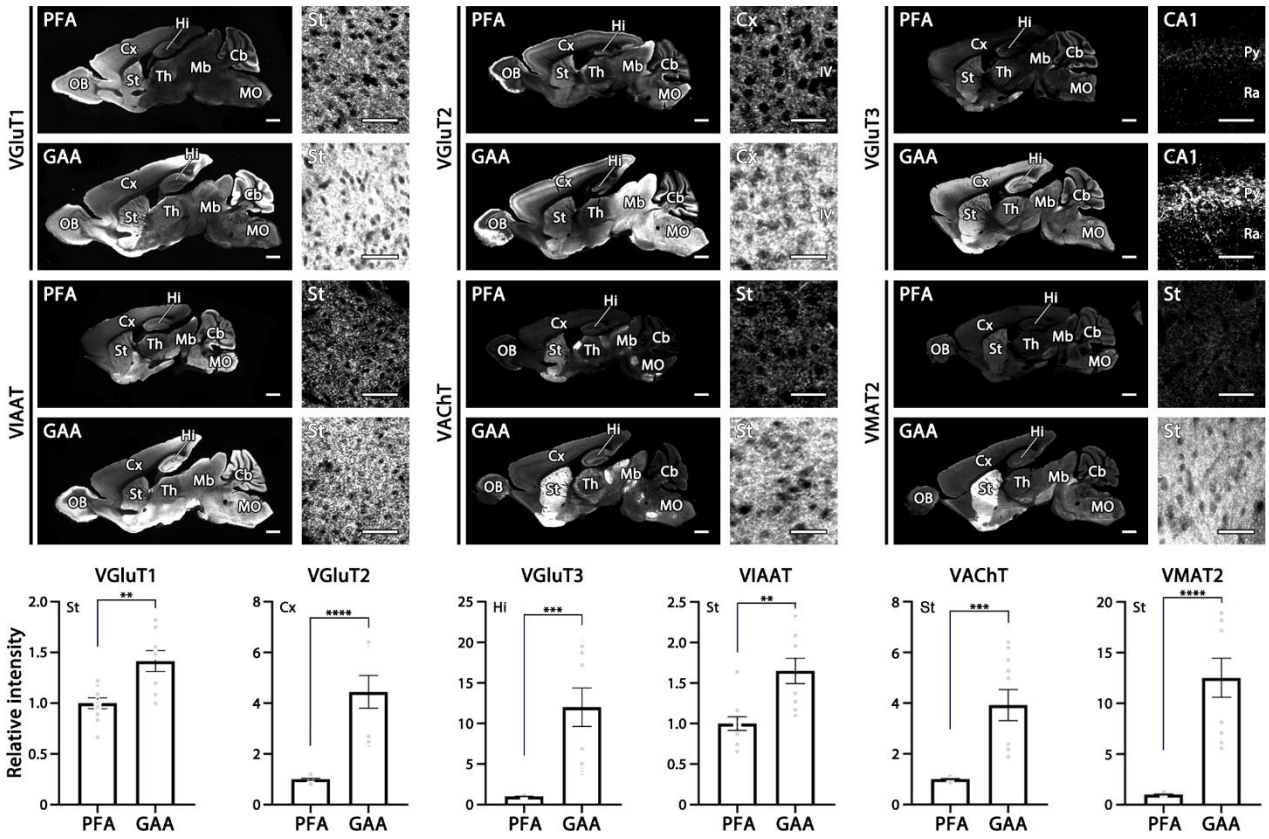

Fig. S12. Vesicular transporters. The mean relative intensity is significantly increased by GAA fixation for vesicular glutamate transporter VGluT1 in the striatum, VGluT2 in the somatosensory cortex, VGluT3 in the hippocampal CA1, vesicular inhibitory amino transporter VIAAT in the striatum, vesicular acetylcholine transporter VAChT in the striatum, and vesicular monoamine transporter VMAT2 in the striatum. Scale bars for high-magnification right panels, 50 μm.

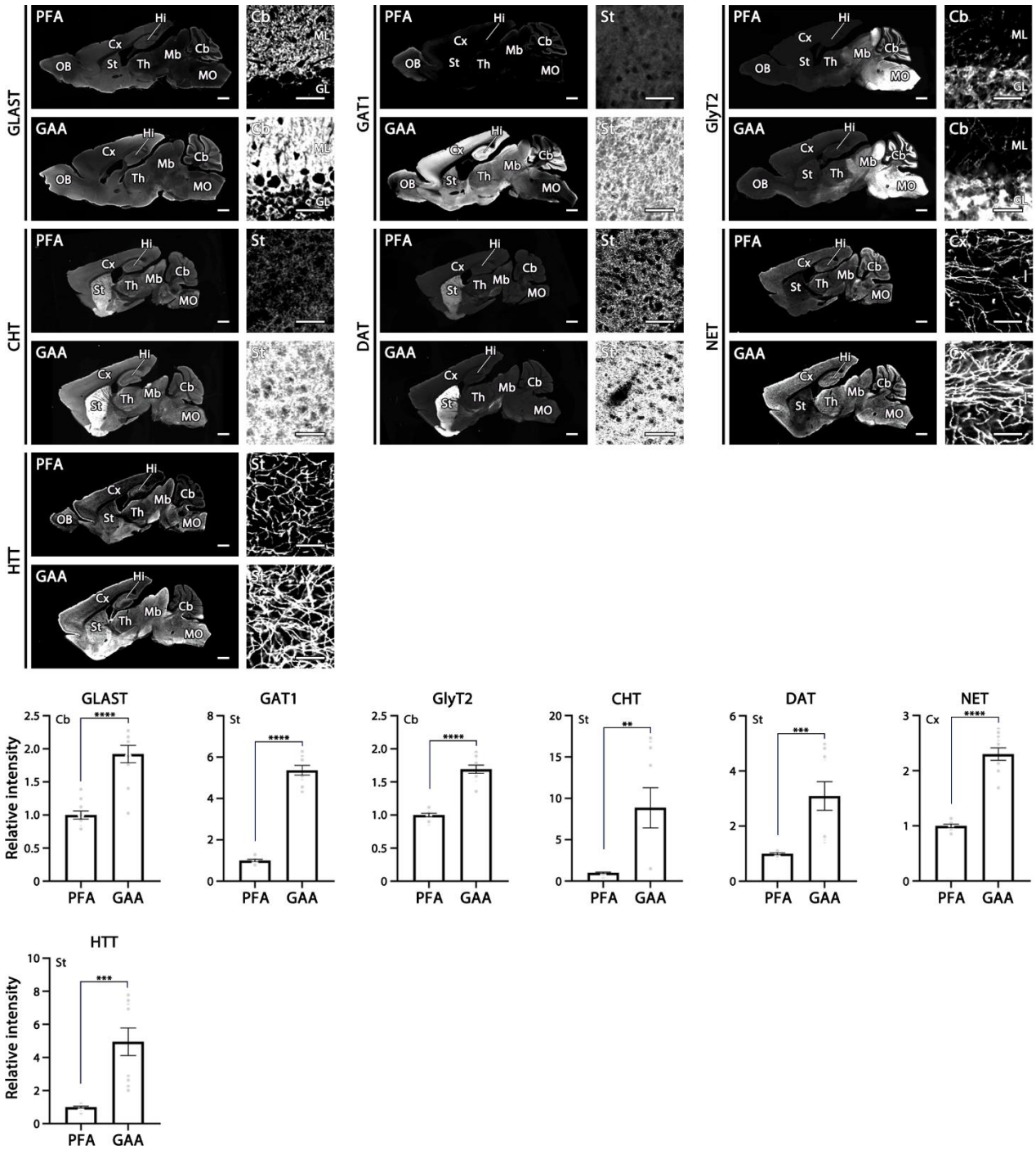

Fig. S13. Plasmalemmal transporters. The mean relative intensity is significantly increased by GAA fixation for glutamate-aspartate transporter GLAST in the cerebellum, GABA transporter GAT1 in the striatum, glycine transporter GlyT2 in the cerebellum, choline transporter CHT in the striatum, dopamine transporter DAT in the striatum, noradrenaline transporter NET in the somatosensory cortex, and serotonin transporter HTT in the striatum. Scale bars for high-magnification right panels, 50 μm.

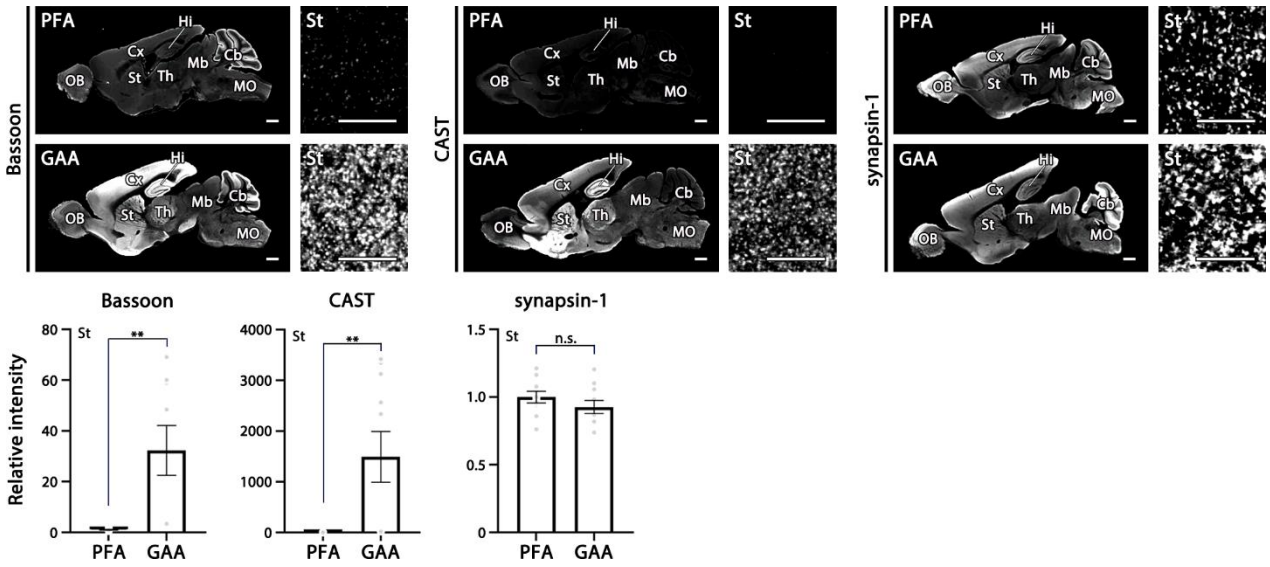

Fig. S14. Synaptic vesicle-associated or active zone proteins. The mean relative intensity is significantly increased by GAA fixation for Bassoon and cytomatrix at the active zone-associated structural protein CAST in the striatum. No significant difference is noted for synapsin-1 in the striatum. Scale bars for high-magnification right panels, 10 μm.

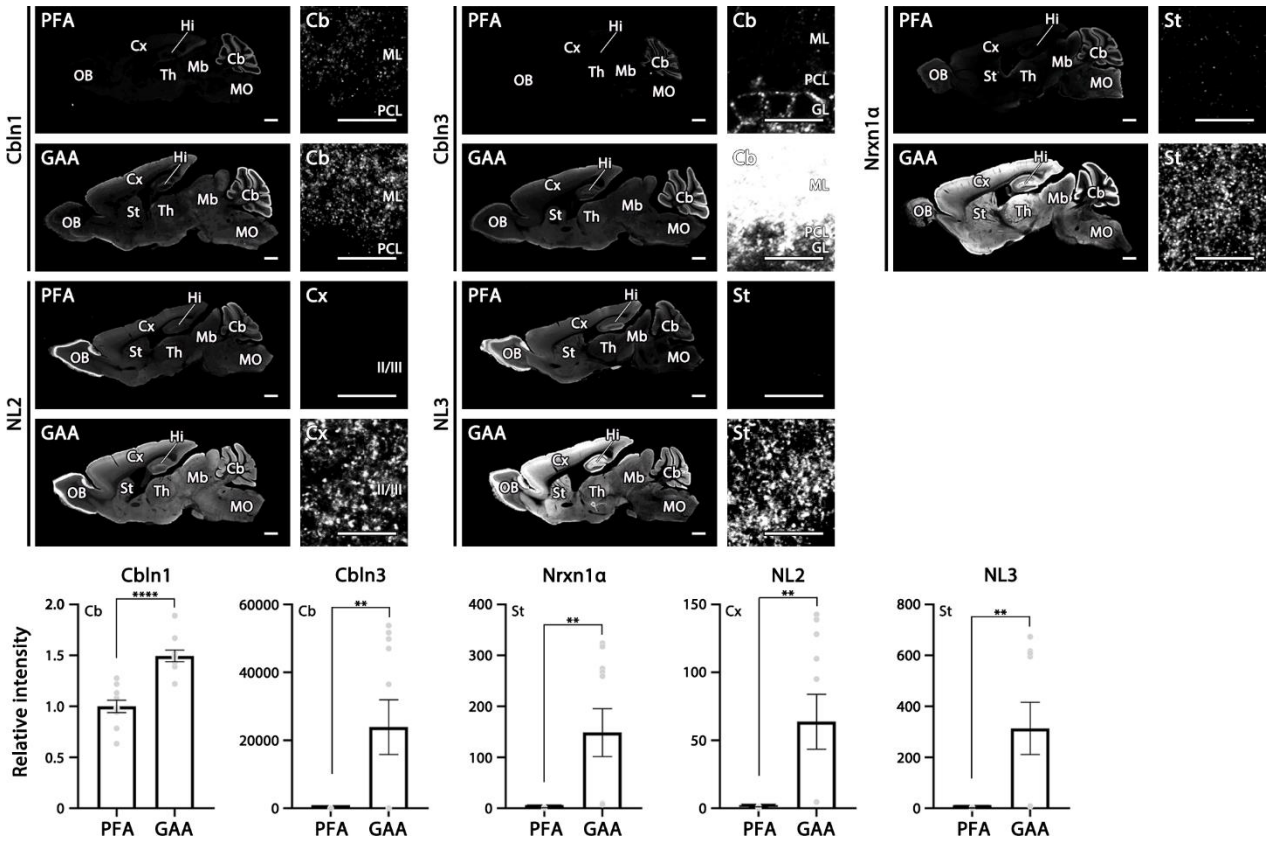

Fig. S15. Synaptic adhesion molecules. The mean relative intensity is significantly increased by GAA fixation for Cbln1 or precerebellin, Cbln3 in the cerebellum, neurexin Nrxn1α in the striatum, Neuroligin (NL)2 in the cortex, and NL3 in the striatum. Scale bars for high-magnification right panels, 10 μm.

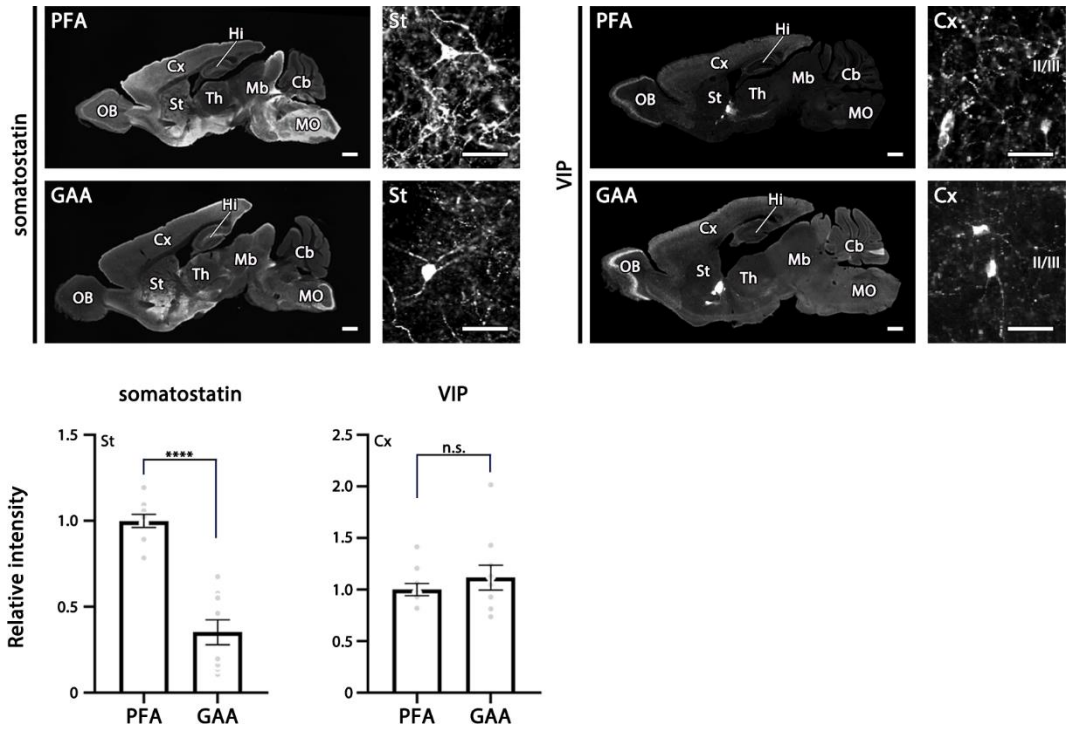

Fig. S16. Neuropeptides. The mean relative intensity is significantly decreased by GAA fixation for somatostatin in the striatum. No significant difference is noted for vasoactive intestinal peptide in the somatosensory cortex. Scale bars for high-magnification right panels, 50 μm.

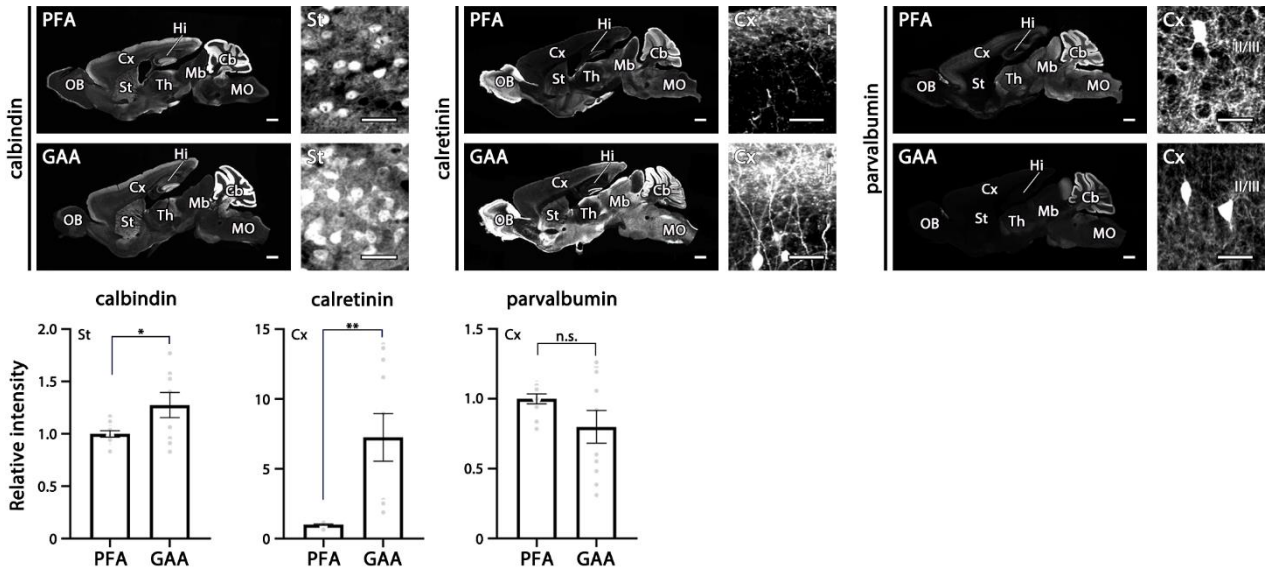

Fig. S17. Cytosolic calcium-binding proteins. The mean relative intensity is significantly increased by GAA fixation for calbindin in the striatum and calretinin in the somatosensory cortex, but not for parvalbumin in the somatosensory cortex. Scale bars for high-magnification right panels, 50 μm.

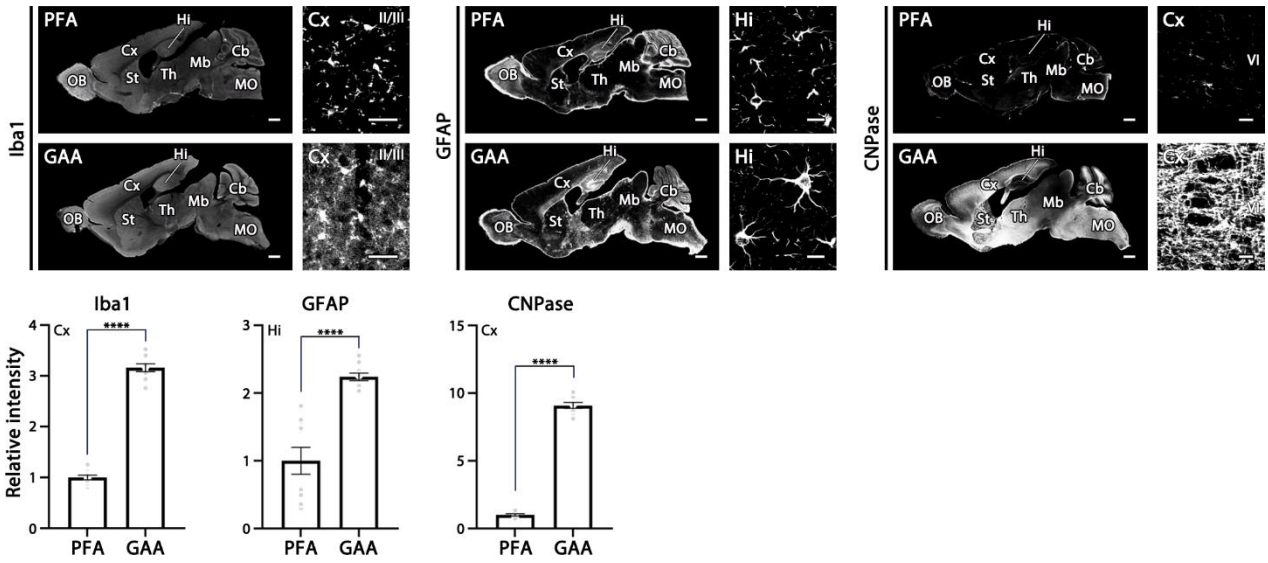

Fig. S18. Glial marker proteins. The mean relative intensity is significantly increased by GAA fixation for microglia marker Iba1, astrocyte marker GFAP in the hippocampal CA1, and oligodendrocyte marker CNPase in the somatosensory cortex. Nevertheless, Iba1 immunoreactivity was more clearly observed in PFA-fixed sections, because non-specific staining appeared in GAA-fixed sections in the somatosensory cortex. Thus, we judged no improvement for Iba1 immunostaining by GAA fixation. Scale bars for high-magnification right panels, 10 μm.

Table S1. List of primary antibodies used in the present study.

Molecules	Sequence (NCBI #)	Host	RRID	Specificity	Source	Figure
ankyrin-G	1708-1726 aa (NP_733924)	Rb	AB_2571661	IB, SL (axon initial segment)	Iwakura et al. (*25*) (MSFR100220)	Figure S10
Bassoon		Ms	AB_11181058	SL (presynapse)	Enzo Life Sciences (VAM-PS003)	Figure S1, S14
calbindin	1-261 aa (NM009788)	Go	AB_2571569	IB	Miura et al. (*31*) (MSFR100410)	Figure S17
		Rb	AB_2571568	IB	Miura et al. (*31*) (MSFR100390)	Figure 4, S6, S7
calretinin	1-271 aa (AB037969)	Rb	AB_2571666	IB	Miyazaki et al. (*32*) (MSFR100450)	Figure S17
CAST	113-161 aa (NM_178085)	Gp	AB_2571671	IB, KO	Uchigashima et al. (*13*) (MSFR100570)	Figure S14
$Ca_V2.1$	421-460 aa (U76716)	Gp	AB_2571851	KO	Miyazaki et al. (*27*) (MSFR106040)	Figure S9
Cbln1	38-52aa (NM019626)	Rb	AB_2571672	KO	Miura et al. (*33*) (MSFR100660)	Figure S15
Cbln3	41-74 aa (NM198114)	Rb	AB_2895273	IB	Iijima et al. (*34*) (MSFR106970)	Figure S15
CHT	531-580 (BC065089)	Go	AB_2571677	IB	Miura et al. (*31*) (MSFR100870)	Figure S13
CNPase		Ms		SL (oligodendrocyte)	Sigma (C5922)	Figure S18
D1R	C-terminus 45 aa (NM010076)	Go	AB_2571594	IB	Narushima et al. (*35*) (MSFR101020)	Figure S11
DAT	1-60 (BC054119)	Gp	AB_2571689	IB	Uchigashima, et al. (*36*) (MSFR101260)	Figure S13
$GABA_A$ Rα1	369–386 (NM_010250)	Rb	AB_2571572	IB	Ichikawa et al. (*37*) (MSFR101530)	Figure 1, 7
$GABA_A$ Rγ2		Rb	AB_2263066	KD	Synaptic Systems (224003)	Figure 6, 7
$GABA_BR2$	858-890aa (NM_001081141)	Gp	AB_2895275	KD	present study	Figure S11
GAT1	564-599aa (NM_178703)	Rb	AB_2571703	IB	Iwakura et al. (*25*) (MSFR101710)	Figure S13
gephyrin		Ms	AB_2232546	SL (inhibitory synapse)	Synaptic Systems (147021)	Figure 1, S10
GFAP	335-400 aa (AF332061)	Rb	AB_2571707	IB, SL (astrocyte)	Hisano et al. (*38*) (MSFR101830)	Figure S18
GLAST	C-terminal 41aa (NM148938)	Rb	AB_2571715	IB, SL (astrocyte)	Shibata et al. (*39*) (MSFR102130)	Figure S13
GluD1	895-932 aa (NM_008166)	Gp	AB_2571759	IB, KO (Fig. 8)	Konno et al. (*15*) (MSFR102510)	Figure 7, 8
GluD2	897-934 aa (D13266)	Rb	AB_2571601	KO (Fig. 8)	Nakamoto et al. (*16*) (MSFR102570)	Figure 5, 7, 8, S5, S8
GluA1-4 (pan-AMPAR)	717-754 aa (X57497)	Gp	AB_2571610	IB	Fukaya et al. (*40*) (MSFR104670)	Figure 2, 4, S6, S7
GluA2	847-863 aa (X57498)	Rb	AB_2571754	IB, KO	Fukaya et al. (*40*) (MSFR102330)	Figure 1, 7
GluA3	853-883 aa (AB022342)	Rb	AB_2571598	IB, KO	Nagy et al. (*41*) (MSFR102360)	Figure 7
GluK2	834-864 aa (D10054)	Rb	AB_2904156	KO lacking the C-terminus	Yan et al. (*42*)	Figure 7

GluN1	909-938 aa (NM_008169)	Rb	AB_2571604	IB, KO (Fig. S4)	Abe et al. (*19*) (MSFR102660)	Figure 3, S4
GluN2B	1301-1456 aa (D10651)	Rb	AB_2571762	IB	Watanabe et al. (*5*) (MSFR102790)	Figure 7
GluN2C	908-927 aa (D10694)	Rb	AB_2571763	IB	Yamada et al. (*21*) (MSFR102810)	Figure 1, 7
GlyT2	1-30aa (AF411042)	Rb	AB_2571606	IB, SL (glycinergic neuron)	Hondo et al. (*43*) (MSFR103070)	Figure S13
Homer-1	1-175 aa (NM_147176)	Rb	AB_2571774	IB	Nakamura et al. (*44*) (MSFR103210)	Figure S10
HTT	1-77 aa (AF013604)	Gp	AB_2571777	IB	Somogyi et al. (*45*) (MSFR103300)	Figure S13
Iba1		Rb	AB_839504	SL (microglia)	FUJIFILM Wako (019-19741)	Figure S18
IP_3R1	2681-2749 (NM010585)	Rb	AB_2571778	IB	Nakamura et al. (*44*) (MSFR103400)	Figure S11
$K_V1.1$	478-492 aa (NM_010595)	Rb	AB_2571787	IB	Iwakura et al. (*25*) (MSFR103610)	Figure S9
mAChR1	229-358 aa (NM007698)	Rb	AB_2571791	IB	Narushima et al. (*46*) (MSFR103750)	Figure S11
mGluR1	945-1127 aa (NM_016976)	Rb	AB_2571799	IB	Tanaka et al. (*47*) (MSFR104040)	Figure S11
NET	1-56 aa (NM_009209)	Go	AB_2571809	IB	Uchigashima et al. (*36*) (MSFR104360)	Figure S13
$Na_V1.1$-1.9 (pan-Na_V)	1492-1508 aa (NM_018733)	Rb	AB_2571818	IB	Iwakura et al. (*25*) (MSFR104700)	Figure S9
NL1	805-826 aa (NM_138666)	Go	AB_2895276	KO (Fig. 6)	present study	Figure 6
NL2	784-829 aa (NM_198862)	Gp	AB_2571609	IB, KO (Fig. 8)	Iwakura et al. (*25*) (MSFR104480)	Figure 8, S15
NL3	739-768 aa (NM_172932)	Gp	AB_2571814	IB, KO (Fig. 8)	Uchigashima et al. (*13*) (MSFR104540)	Figure 8, S15
Nrxn1α	1454–1507 aa (NM_020252)	Rb	AB_2571817	IB	Uchigashima et al. (*13*) (MSFR104640)	Figure S15
parbalbumin	whole sequence (NM013645)	Gp	AB_2571615	IB	Nakamura et al. (*44*) (MSFR105260)	Figure S4, S17
PLCβ1	36-87 aa (NM_019677)	Gp	AB_2571828	IB, KO	Fukaya et al. (*48*) (MSFR104930)	Figure S11
somatostatin	35-88aa (BC010770)	Rb	AB_2895277	ISH	present study	Figure S16
PSD-95	1–64 (D50621)	Gp	AB_2571612	IB, KO (Fig. 8)	Fukaya & Watanabe (*8*) (MSFR105190)	Figure 1, 6, 8, S2, S3
		Go	AB_2920798	IB	Fukaya & Watanabe (*8*) (MSFR107520)	Figure S4
SAP-102	1-146 aa (D87117)	Rb	AB_2571832	IB	Fukaya & Watanabe (*8*) (MSFR105070)	Figure S3
Shank2	C-terminal 13 aa (NM_001081370)	Rb	AB_2571839	IB	Matsuda et al. (*49*) (MSFR105500)	Figure S10
synapsin-1	686-706aa (NM_013680)	Rb	AB_2636934	IB	present study	Figure S14
TARP-γ2	302-318 aa (AF077739)	Gp	AB_2895281	KO	Yamazaki et al. (*26*) (MSFR105780)	Figure S10
TARP-γ8	362-421aa (AF361350)	Rb	AB_2571846	KO	Fukaya et al. (*40*) (MSFR105830)	Figure S10
VAChT	518-530 aa (AF019045)	Rb	AB_2736903	IB	Nakamura et al. (*44*) (MSFR106490)	Figure S12

VGluT1	531–560 aa (BC054462)	Go	AB_2571617	IB	Miyazaki et al. (*12*) (MSFR106210)	Figure 1, 5, S1, S12
VGluT2	559–582 aa (BC038375)	Gp	AB_2571621	IB	Miyazaki et al. (*12*) (MSFR107440**)**	Figure 2, 5, S1, S12
		Go	AB_2571620	IB	Kawamura et al. (*50*) (MSFR106270)	Figure 4, S6, S7
VGluT3	558–602 aa (AF510321)	Go	AB_2571854	IB	Somogyi et al. (*45*) (MSFR106340)	Figure S12
VIAAT	31–112 (BC052020)	Rb	AB_2571622	IB	Miura et al. (*31*) (MSFR106120)	Figure S1, S12
VIP	58-72aa (XM_006512446)	Gp	AB_2895283	ISH	present study	Figure S16
VMAT2	468-515 aa (L00603)	Rb	AB_2571857	IB	Somogyi et al. (*45*) (MSFR106410)	Figure S12

Table S2. Detailed data and statistics.

Figures									
		Number of measured areas	Mean ± SEM	Statistics	Result	Post-hoc Test	Comparison	Significance	P-value
Fig.1A GluA2	PFA	10	1.00 ± 0.22	One-way ANOVA	F (4, 45) = 5.405		PFA, G, GAA, GE, GAAE	**	$P = 0.0012$
	G	10	118.21 ± 32.42			Dunnett's test	PFA G	**	$P = 0.0038$
	GAA	10	127.23 ± 35.28				PFA GAA	**	$P = 0.0017$
	GE	10	29.42 ± 9.07				PFA GE	n.s.	$P = 0.8089$
	GAAE	10	73.67 ± 20.09				PFA GAAE	n.s.	$P = 0.1097$
Fig.1A $GABA_AR\alpha1$	PFA	10	1.00 ± 0.04	One-way ANOVA	F (4, 45) = 13.94		PFA, G, GAA, GE, GAAE	****	$P_{adj} < 0.0001$
	G	10	6.05 ± 1.11			Dunnett's test	PFA G	***	$P = 0.0002$
	GAA	10	6.96 ± 1.36				PFA GAA	****	$P_{adj} < 0.0001$
	GE	10	0.56 ± 0.15				PFA GE	n.s.	$P = 0.9841$
	GAAE	10	2.27 ± 0.12				PFA GAAE	n.s.	$P = 0.6192$
Fig.1A PSD-95	PFA	10	1.00 ± 0.07	One-way ANOVA	F (4, 45) = 56.63		PFA, G, GAA, GE, GAAE	****	$P_{adj} < 0.0001$
	G	10	4.15 ± 0.31			Dunnett's test	PFA G	****	$P_{adj} < 0.0001$
	GAA	10	6.35 ± 0.73				PFA GAA	****	$P_{adj} < 0.0001$
	GE	10	0.25 ± 0.03				PFA GE	n.s.	$P = 0.3855$
	GAAE	10	0.48 ± 0.03				PFA GAAE	n.s.	$P = 0.6991$
Fig.1A gephyrin	PFA	10	1.00 ± 0.14	One-way ANOVA	F (4, 45) = 13.44		PFA, G, GAA, GE, GAAE	****	$P_{adj} < 0.0001$
	G	10	10.83 ± 1.84			Dunnett's test	PFA G	****	$P_{adj} < 0.0001$
	GAA	10	14.30 ± 1.38				PFA GAA	****	$P_{adj} < 0.0001$
	GE	10	9.63 ± 1.51				PFA GE	***	$P = 0.0002$
	GAAE	10	9.48 ± 1.15				PFA GAAE	***	$P = 0.0002$
Fig.1C		PFA_PBS (6), PFA_PBS-T (6), GAA_PBS (6), GAA_PBS-T (6)	PFA_PBS-T/PFA_PBS (1.54 ± 0.10), GAA_PBS-T/GAA_PBS (4.27 ± 0.14)	Unpaired t-test	t = 15.99, df = 10 (Two-tailed)		PFA GAA	****	$P_{adj} < 0.0001$
Fig.2	VGluT2	PFA (10), GAA (10)	PFA (1.00 ± 0.13), GAA (11.35 ± 1.01)	Unpaired t-test	t = 10.13, df = 18 (Two-tailed)		PFA GAA	****	$P_{adj} < 0.0001$

	AMPAR	PFA (10), GAA (10)	PFA (1.00 ± 0.37), GAA (9199.67 ± 460.57)	Unpaired t-test	t = 19.97, df = 18 (Two-tailed)	PFA GAA	****	P_{adj} < 0.0001
Fig. 3G	CA1 Or	PFA (6), GAA (6)	PFA (1.00 ± 0.06), GAA (8.73 ± 0.64)	Unpaired t-test	t = 12.03, df = 10 (Two-tailed)	PFA GAA	****	P_{adj} < 0.0001
	CA1 Ra	PFA (6), GAA (6)	PFA (1.00 ± 0.04), GAA (10.03 ± 0.53)	Unpaired t-test	t = 16.98, df = 10 (Two-tailed)	PFA GAA	****	P_{adj} < 0.0001
Fig. 3J		PFA (66 synapses), GAA (62 synapses)	PFA (0.00 ± 0.00), GAA (5.54 ± 0.45)	Unpaired t-test	t = 12.68, df = 126 (Two-tailed)	PFA GAA	****	P_{adj} < 0.0001
Fig. 4I	0 µm	6	1.00 ± 0.03	One-way ANOVA	F (9, 50) = 283.6	0, 0.2, 0.4, 0.6, 0.8, 1.0, 1.2, 1.4, 1.6, 1.8 µm	****	P_{adj} < 0.0001
	0.2 µm	6	0.89 ± 0.04		Dunnett's test	0 µm 0.2 µm	*	P = 0.0159
	0.4 µm	6	0.69 ± 0.04			0 µm 0.4 µm	****	P_{adj} < 0.0001
	0.6 µm	6	0.45 ± 0.03			0 µm 0.6 µm	****	P_{adj} < 0.0001
	0.8 µm	6	0.25 ± 0.01			0 µm 0.8 µm	****	P_{adj} < 0.0001
	1.0 µm	6	0.10 ± 0.01			0 µm 1.0 µm	****	P_{adj} < 0.0001
	1.2 µm	6	0.04 ± 0.01			0 µm 1.2 µm	****	P_{adj} < 0.0001
	1.4 µm	6	0.02 ± 0.01			0 µm 1.4 µm	****	P_{adj} < 0.0001
	1.6 µm	6	0.00 ± 0.00			0 µm 1.6 µm	****	P_{adj} < 0.0001
	1.8 µm	6	0.00 ± 0.00			0 µm 1.8 µm	****	P_{adj} < 0.0001
Fig. 4J	0 µm	6	1.00 ± 0.04	One-way ANOVA	F (9, 50) = 0.352	0, 0.2, 0.4, 0.6, 0.8, 1.0, 1.2, 1.4, 1.6, 1.8 µm	n.s.	P = 0.9520
	0.2 µm	6	0.97 ± 0.06					
	0.4 µm	6	1.04 ± 0.06					
	0.6 µm	6	1.00 ± 0.05					
	0.8 µm	6	1.07 ± 0.05					
	1.0 µm	6	1.06 ± 0.06					
	1.2 µm	6	1.05 ± 0.05					
	1.4 µm	6	1.02 ± 0.05					
	1.6 µm	6	0.98 ± 0.06					
	1.8 µm	6	0.98 ± 0.07					

Fig. 4K PFA	0 µm	AMPAR(+)VGluT2(+)/Total VGluT2(+): 61/64	Apposition rate: 95.31%					
	0.2 µm	98/104	94.23%					
	0.4 µm	108/127	85.04%					
	0.6 µm	93/143	65.03%					
	0.8 µm	76/159	47.79%					
	1.0 µm	33/163	20.25%					
	1.2 µm	9/166	5.42%					
	1.4 µm	3/172	1.74%					
	1.6 µm	3/159	1.89%					
	1.8 µm	3/150	2.00%					
Fig. 4K GAA	0 µm	80/82	97.56%					
	0.2 µm	105/108	97.22%					
	0.4 µm	122/130	93.85%					
	0.6 µm	138/144	95.83%					
	0.8 µm	153/161	95.03%					
	1.0 µm	153/162	94.44%					
	1.2 µm	157/169	92.90%					
	1.4 µm	160/177	90.40%					
	1.6 µm	153/176	86.93%					
	1.8 µm	135/167	80.84%					
Fig. 5E		PFA (159 synapses), GAA (32 synapses)	PFA (9.64 ± 0.53), GAA (19.81 ± 1.92)	Unpaired t-test	t = 6.955, df = 189 (Two-tailed)		PFA GAA	****	P_{adj} < 0.0001
Fig. 6G CA1 (Ra)	PFA WT	10	1.00 ± 0.03	One-way ANOVA	F (3, 36) = 1683		PFA-WT, PFA-KO, GAA-WT, GAA-KO	****	P_{adj} < 0.0001
	PFA KO	10	0.01 ± 0.00			Tukey's test	PFA-WT PFA-KO	****	P_{adj} < 0.0001
	GAA WT	10	4.24 ± 0.07				GAA-WT GAA-KO	****	P_{adj} < 0.0001

	GAA KO	10	0.28 ± 0.05			PFA-WT GAA-WT	****	P_{adj} < 0.0001
Fig. 6G CA1 (LM)	PFA WT	10	1.00 ± 0.04	One-way ANOVA	F (3, 36) = 980.3	PFA-WT, PFA-KO, GAA-WT, GAA-KO	****	P_{adj} < 0.0001
	PFA KO	10	0.02 ± 0.00		Tukey's test	PFA-WT PFA-KO	****	P_{adj} < 0.0001
	GAA WT	10	4.47 ± 0.11			GAA-WT GAA-KO	****	P_{adj} < 0.0001
	GAA KO	10	0.18 ± 0.06			PFA-WT GAA-WT	****	P_{adj} < 0.0001
Fig. 6G Cx	PFA WT	10	1.00 ± 0.02	One-way ANOVA	F(3, 36) =707.8	PFA-WT, PFA-KO, GAA-WT, GAA-KO	****	P_{adj} < 0.0001
	PFA KO	10	0.08 ± 0.01		Tukey's test	PFA-WT PFA-KO	****	P_{adj} < 0.0001
	GAA WT	10	2.35 ± 0.07			GAA-WT GAA-KO	****	P_{adj} < 0.0001
	GAA KO	10	0.08 ± 0.03			PFA-WT GAA-WT	****	P_{adj} < 0.0001
Fig. 6G St	PFA WT	10	1.00 ± 0.06	One-way ANOVA	F (3, 36) =177.8	PFA-WT, PFA-KO, GAA-WT, GAA-KO	****	P_{adj} < 0.0001
	PFA KO	10	0.29 ± 0.03		Tukey's test	PFA-WT PFA-KO	****	P_{adj} < 0.0001
	GAA WT	10	2.28 ± 0.13			GAA-WT GAA-KO	****	P_{adj} < 0.0001
	GAA KO	10	0.11 ± 0.02			PFA-WT GAA-WT	****	P_{adj} < 0.0001
Fig. 6L	CA1 Ra	PSD-95 (12 area, 1567 clusters), GABAARα1 (12, 1049)	PSD-95 (1.00 ± 0.01), GABAARα1 (0.94 ± 0.02)	Unpaired t-test	t = 1.122, df = 22 (Two-tailed)	PSD-95 GABAARα1	n.s.	P = 0.2740
Fig. 6M	CA1 LM	PSD-95 (12, 1801), GABAARα1 (12, 1436)	PSD-95 (1.00 ± 0.01), GABAARα1 (0.63 ± 0.01)	Unpaired t-test	t = 7.734, df = 22 (Two-tailed)	PSD-95 GABAARα1	****	P_{adj} < 0.0001
Fig. 6N	Cx LI	PSD-95 (12, 1346), GABAARα1 (12, 1186)	PSD-95 (1.00 ± 0.01), GABAARα1 (0.79 ± 0.01)	Unpaired t-test	t = 3.396, df = 22 (Two-tailed)	PSD-95 GABAARα1	**	P = 0.0026
Fig. 6O	Cx LV	PSD-95 (12, 1393), GABAARα1 (12, 741)	PSD-95 (1.00 ± 0.01), GABAARα1 (0.72 ± 0.01)	Unpaired t-test	t = 4.568, df = 22 (Two-tailed)	PSD-95 GABAARα1	***	P = 0.0002
Fig. 6S		WT (37 synapses), NL1-KO (69 synapses)	WT (3.16 ± 0.22), NL1-KO (0.03 ± 0.03)	Unpaired t-test	t = 19.20, df = 104 (Two-tailed)	WT NL1-KO	****	P_{adj} < 0.0001
Fig. 7	GluA2	PFA (10), GAA (10)	PFA (1.00 ± 0.17), GAA (193.22 ± 59.99)	Unpaired t-test	t = 3.204, df = 18 (Two-tailed)	PFA GA	**	P = 0.0049
	GluA3	PFA (10), GAA (10)	PFA (1.00 ± 0.14), GAA (8.82 ± 2.26)	Unpaired t-test	t = 3.453, df = 18 (Two-tailed)	PFA GAA	**	P = 0.0028

	GluK2	PFA (10), GAA (10)	PFA (1.00 ± 0.21), GAA (1475.42 ± 499.42)	Unpaired t-test	t = 2.952, df = 18 (Two-tailed)	PFA GAA	**	P = 0.0085
	GluN2B	PFA (10), GAA (10)	PFA (1.00 ± 0.19), GAA (283.73 ± 69.75)	Unpaired t-test	t = 4.053, df = 18 (Two-tailed)	PFA GAA	***	P = 0.0007
	GluN2C	PFA (10), GAA (10)	PFA (1.00 ± 0.14), GAA (75.72 ± 5.11)	Unpaired t-test	t = 14.63, df = 18 (Two-tailed)	PFA GAA	****	P_{adj} < 0.0001
	GluD1	PFA (10), GAA (10)	PFA (1.00 ± 0.08), GAA (3.60 ± 0.15)	Unpaired t-test	t = 15.41, df = 18 (Two-tailed)	PFA GAA	****	P_{adj} < 0.0001
	GluD2	PFA (10), GAA (10)	PFA (1.00 ± 0.17), GAA (13.00 ± 0.42)	Unpaired t-test	t = 26.63, df = 18 (Two-tailed)	PFA GAA	****	P_{adj} < 0.0001
	$GABA_A$ Rα1	PFA (10), GAA (10)	PFA (1.00 ± 0.05), GAA (10.48 ± 2.84)	Unpaired t-test	t = 3.331, df = 18 (Two-tailed)	PFA GAA	**	P = 0.0037
	$GABA_A$ Rγ2	PFA (10), GAA (10)	PFA (1.00 ± 0.28), GAA (709.20 ± 227.75)	Unpaired t-test	t = 3.110, df = 18 (Two-tailed)	PFA GAA	**	P = 0.0061
Supplementary Figures								
Fig.S1A Bassoon	PFA	10	1.00 ± 0.05	One-way ANOVA	F (4, 45) = 15.92	PFA, G, GAA, GE, GAAE	****	P_{adj} < 0.0001
	G	10	3.71 ± 0.58		Dunnett's test	PFA G	****	P_{adj} < 0.0001
	GAA	10	4.52 ± 0.41			PFA GAA	****	P_{adj} < 0.0001
	GE	10	2.69 ± 0.06			PFA GE	**	P = 0.0027
	GAAE	10	3.08 ± 0.19			PFA GAAE	***	P = 0.0002
Fig.S1A VGluT1	PFA	10	1.00 ± 0.05	One-way ANOVA	F (4, 45) = 31.68	PFA, G, GAA, GE, GAAE	****	P_{adj} < 0.0001
	G	10	3.79 ± 0.10		Dunnett's test	PFA G	****	P_{adj} < 0.0001
	GAA	10	3.28 ± 0.16			PFA GAA	****	P_{adj} < 0.0001
	GE	10	3.08 ± 0.35			PFA GE	****	P_{adj} < 0.0001
	GAAE	10	3.15 ± 0.13			PFA GAAE	****	P_{adj} < 0.0001
Fig.S1A VGluT2	PFA	10	1.00 ± 0.08	One-way ANOVA	F (4, 45) = 5.237	PFA, G, GAA, GE, GAAE	**	P = 0.0015
	G	10	18.18 ± 4.76		Dunnett's test	PFA G	***	P = 0.0009
	GAA	10	15.84 ± 4.17			PFA GAA	**	P = 0.0044
	GE	10	7.78 ± 1.85			PFA GE	n.s.	P = 0.3340
	GAAE	10	7.64 ± 1.59			PFA GAAE	n.s.	P = 0.3518
Fig.S1A VIAAT	PFA	10	1.00 ± 0.02	One-way ANOVA	F (4, 45) = 26.48	PFA, G, GAA, GE, GAAE	****	P_{adj} < 0.0001

	G	10	2.78 ± 0.16			Dunnett's test	PFA G	****	P_{adj} < 0.0001
	GAA	10	2.43 ± 0.20				PFA GAA	****	P_{adj} < 0.0001
	GE	10	1.59 ± 0.09				PFA GE	*	P = 0.0176
	GAAE	10	1.48 ± 0.17				PFA GAAE	n.s.	P = 0.0667
Fig. S2F Cx	PFA	6	1.00 ± 0.02	One-way ANOVA	F (4, 25) = 174.8		PFA, 3G0.8A, 3G8A, 9G0.8A, 9G8A	****	P_{adj} < 0.0001
	3G 0.8A	6	3.90 ± 0.11			Tukey's test	PFA 3G0.8A	****	P_{adj} < 0.0001
	3G 8A	6	3.71 ± 0.07				PFA 3G8A	****	P_{adj} < 0.0001
	9G 0.8A	6	3.85 ± 0.14				PFA 9G0.8A	****	P_{adj} < 0.0001
	9G 8A	6	4.05 ± 0.10				PFA 9G8A	****	P_{adj} < 0.0001
Fig. S2F St	PFA	6	1.00 ± 0.04	One-way ANOVA	F (4, 25) = 11.40		PFA, 3G0.8A, 3G8A, 9G0.8A, 9G8A	****	P_{adj} < 0.0001
	3G 0.8A	6	2.99 ± 0.22			Tukey's test	PFA 3G0.8A	****	P_{adj} < 0.0001
	3G 8A	6	2.42 ± 0.36				PFA 3G8A	**	P = 0.0037
	9G 0.8A	6	2.89 ± 0.22				PFA 9G0.8A	***	P = 0.0001
	9G 8A	6	2.92 ± 0.28				PFA 9G8A	****	P_{adj} < 0.0001
Fig. S3D PSD-95	Cx			One-way ANOVA	F (2, 27) = 377.0		4%PFA, 1%PFA, GAA	****	P_{adj} < 0.0001
	4% PFA	10	1.00 ± 0.05			Tukey's test	4%PFA 1%PFA	***	P = 0.0003
	1% PFA	10	1.53 ± 0.03				4%PFA GAA	****	P_{adj} < 0.0001
	GAA	10	4.02 ± 0.13				1%PFA GAA	****	P_{adj} < 0.0001
	St			One-way ANOVA	F(2, 27) = 162.3		4%PFA, 1%PFA, GAA	****	P_{adj} < 0.0001
	4% PFA	10	1.00 ± 0.04			Tukey's test	4%PFA 1%PFA	n.s.	P = 0.9011
	1% PFA	10	1.07 ± 0.04				4%PFA GAA	****	P_{adj} < 0.0001
	GAA	10	3.51 ± 0.19				1%PFA GAA	****	P_{adj} < 0.0001
Fig. S3H SAP-102	Cx			One-way ANOVA	F (2, 27) = 484.1		4%PFA, 1%PFA, GAA	****	P_{adj} < 0.0001
	4% PFA	10	1.00 ± 0.03			Tukey's test	4%PFA 1%PFA	****	P_{adj} < 0.0001
	1% PFA	10	1.65 ± 0.05				4%PFA GAA	****	P_{adj} < 0.0001
	GAA	10	2.97 ± 0.05				1%PFA GAA	****	P_{adj} < 0.0001
	Hi			One-way ANOVA	F (2, 27) = 570.9		4%PFA, 1%PFA, GAA	****	P_{adj} < 0.0001
	4% PFA	10	1.00 ± 0.08			Tukey's test	4%PFA 1%PFA	n.s.	P = 0.2041

	1% PFA	10	1.29 ± 0.04			4%PFA GAA	****	P_{adj} < 0.0001
	GAA	10	6.00 ± 0.18			1%PFA GAA	****	P_{adj} < 0.0001
Fig. S5D		PFA (6), GAA (6)	PFA (1.00 ± 0.06), GAA (4.41 ± 0.81)	Unpaired t-test	t = 4.201, df = 10 (Two-tailed)	PFA GAA	**	*P* = 0.0018
Fig. S8E		PFA (6), GAA (6)	PFA (1.00 ± 0.08), GAA (4.25 ± 0.96)	Unpaired t-test	t = 3.359, df = 10 (Two-tailed)	PFA GAA	**	*P* = 0.0073
Fig. S8F	GluD2 clusters /100 μm^2	PFA (6), GAA (6)	PFA (0.12 ± 0.01), GAA (0.14 ± 0.01)	Unpaired t-test	t = 2.016, df = 10 (Two-tailed)	PFA GAA	n.s.	*P* = 0.0715
	Size of clusters (100 μm^2)	PFA (6), GAA (6)	PFA (0.63 ± 0.09), GAA (2.49 ± 0.491)	Unpaired t-test	t = 3.739, df = 10 (Two-tailed)	PFA GAA	**	*P* = 0.0039
Fig. S9	Nav1.1-1.9	PFA (10), GAA (10)	PFA (1.00 ± 0.18), GAA (85.61 ± 27.96)	Unpaired t-test	t = 3.026, df = 18 (Two-tailed)	PFA GAA	**	*P* = 0.0073
	Kv1.1	PFA (10), GAA (10)	PFA (1.00 ± 0.04), GAA (12.41 ± 1.05)	Unpaired t-test	t = 10.86, df = 18 (Two-tailed)	PFA GAA	****	P_{adj} < 0.0001
	Cav2.1	PFA (10), GAA (10)	PFA (1.00 ± 0.12), GAA (16.81 ± 4.65)	Unpaired t-test	t = 3.399, df = 18 (Two-tailed)	PFA GAA	**	*P* = 0.0032
Fig. S10	TARP-γ2	PFA (10), GAA (10)	PFA (1.00 ± 0.04), GAA (22.03 ± 6.42)	Unpaired t-test	t = 3.275, df = 18 (Two-tailed)	PFA GAA	**	*P* = 0.0042
	TARP-γ8	PFA (10), GAA (10)	PFA (1.00 ± 0.04), GAA (3.37 ± 0.35)	Unpaired t-test	t = 6.702, df = 18 (Two-tailed)	PFA GAA	****	P_{adj} < 0.0001
	Shank2	PFA (10), GAA (10)	PFA (1.00 ± 0.05), GAA (5.06 ± 0.79)	Unpaired t-test	t = 5.156, df = 18 (Two-tailed)	PFA GAA	****	P_{adj} < 0.0001
	Homer-1	PFA (10), GAA (10)	PFA (1.00 ± 0.05), GAA (2.81 ± 0.20)	Unpaired t-test	t = 8.811, df = 18 (Two-tailed)	PFA GAA	****	P_{adj} < 0.0001
	gephyrin	PFA (10), GAA (10)	PFA (1.00 ± 0.07), GAA (3.99 ± 0.42)	Unpaired t-test	t = 6.955, df = 18 (Two-tailed)	PFA GAA	****	P_{adj} < 0.0001
	ankyrin-G	PFA (10), GAA (10)	PFA (1.00 ± 0.03), GAA (3.71 ± 0.39)	Unpaired t-test	t = 6.936, df = 18 (Two-tailed)	PFA GAA	****	P_{adj} < 0.0001
Fig. S11	mGluR1	PFA (10), GAA (10)	PFA (1.00 ± 0.04), GAA (0.85 ± 0.12)	Unpaired t-test	t = 1.250, df = 18 (Two-tailed)	PFA GAA	n.s.	*P* = 0.2271
	$GABA_BR2$	PFA (10), GAA (10)	PFA (1.00 ± 0.02), GAA (9.65 ± 2.37)	Unpaired t-test	t = 3.648, df = 18 (Two-tailed)	PFA GAA	**	*P* = 0.0018
	mAChR1	PFA (10), GAA (10)	PFA (1.00 ± 0.02), GAA (0.95 ± 0.13)	Unpaired t-test	t = 0.3863, df = 18 (Two-tailed)	PFA GAA	n.s.	*P* = 0.7038
	D1R	PFA (10), GAA (10)	PFA (1.00 ± 0.05), GAA (2.70 ± 0.31)	Unpaired t-test	t = 5.416, df = 18 (Two-tailed)	PFA GAA	****	P_{adj} < 0.0001

	IP_3R1	PFA (10), GAA (10)	PFA (1.00 ± 0.40), GAA (17519.80 ± 717.84)	Unpaired t-test	t = 24.40, df = 18 (Two-tailed)	PFA GAA	****	P_{adj} < 0.0001
	PLCβ1	PFA (10), GAA (10)	PFA (1.00 ± 0.09), GAA (52.08 ± 6.68)	Unpaired t-test	t = 7.641, df = 18 (Two-tailed)	PFA GAA	****	P_{adj} < 0.0001
Fig. S12	VGluT1	PFA (10), GAA (10)	PFA (1.00 ± 0.05), GAA (1.42 ± 0.10)	Unpaired t-test	t = 3.556, df = 18 (Two-tailed)	PFA GAA	**	*P* = 0.0023
	VGluT2	PFA (10), GAA (10)	PFA (1.00 ± 0.03), GAA (4.45 ± 0.65)	Unpaired t-test	t = 5.332, df = 18 (Two-tailed)	PFA GAA	****	P_{adj} < 0.0001
	VGluT3	PFA (10), GAA (10)	PFA (1.00 ± 0.04), GAA (12.01 ± 2.38)	Unpaired t-test	t = 4.624, df = 18 (Two-tailed)	PFA GAA	***	*P* = 0.0002
	VIAAT	PFA (10), GAA (10)	PFA (1.00 ± 0.08), GAA (1.65 ± 0.16)	Unpaired t-test	t = 3.653, df = 18 (Two-tailed)	PFA GAA	**	*P* = 0.0018
	VAChT	PFA (10), GAA (10)	PFA (1.00 ± 0.02), GAA (3.92 ± 0.61)	Unpaired t-test	t = 4.762, df = 18 (Two-tailed)	PFA GAA	***	*P* = 0.0002
	VMAT2	PFA (10), GAA (10)	PFA (1.00 ± 0.04), GAA (12.53 ± 1.93)	Unpaired t-test	t = 5.973, df = 18 (Two-tailed)	PFA GAA	****	P_{adj} < 0.0001
Fig. S13	GLAST	PFA (10), GAA (10)	PFA (1.00 ± 0.06), GAA (1.92 ± 0.13)	Unpaired t-test	t = 6.373, df = 18 (Two-tailed)	PFA GAA	****	P_{adj} < 0.0001
	GAT1	PFA (10), GAA (10)	PFA (1.00 ± 0.06), GAA (5.37 ± 0.24)	Unpaired t-test	t = 18.06, df = 18 (Two-tailed)	PFA GAA	****	P_{adj} < 0.0001
	GlyT2	PFA (10), GAA (10)	PFA (1.00 ± 0.03), GAA (1.69 ± 0.06)	Unpaired t-test	t = 10.12, df = 18 (Two-tailed)	PFA GAA	****	P_{adj} < 0.0001
	CHT	PFA (10), GAA (10)	PFA (1.00 ± 0.08), GAA (8.86 ± 2.43)	Unpaired t-test	t = 3.234, df = 18 (Two-tailed)	PFA GAA	**	*P* = 0.0046
	DAT	PFA (10), GAA (10)	PFA (1.00 ± 0.03), GAA (3.09 ± 0.52)	Unpaired t-test	t = 4.007, df = 18 (Two-tailed)	PFA GAA	***	*P* = 0.0008
	NET	PFA (10), GAA (10)	PFA (1.00 ± 0.03), GAA (2.30 ± 0.11)	Unpaired t-test	t = 10.98, df = 18 (Two-tailed)	PFA GAA	****	P_{adj} < 0.0001
	HTT	PFA (10), GAA (10)	PFA (1.00 ± 0.05), GAA (4.96 ± 0.83)	Unpaired t-test	t = 4.735, df = 18 (Two-tailed)	PFA GAA	***	*P* = 0.0002
Fig. S14	Bassoon	PFA (10), GAA (10)	PFA (1.00 ± 0.17), GAA (32.33 ± 9.81)	Unpaired t-test	t = 3.192, df = 18 (Two-tailed)	PFA GAA	**	*P* = 0.0050
	CAST	PFA (10), GAA (10)	PFA (1.00 ± 0.28), GAA (1490.61 ± 500.46)	Unpaired t-test	t = 2.976, df = 18 (Two-tailed)	PFA GAA	**	*P* = 0.0081
	synapsin-1	PFA (10), GAA (10)	PFA (1.00 ± 0.04), GAA (0.93 ± 0.05)	Unpaired t-test	t = 1.137, df = 18 (Two-tailed)	PFA GAA	n.s.	*P* = 0.2703
Fig. S15	Cbln1	PFA (10), GAA (10)	PFA (1.00 ± 0.06), GAA (1.50 ± 0.06)	Unpaired t-test	t = 5.948, df = 18 (Two-tailed)	PFA GAA	****	P_{adj} < 0.0001

	Cbln3	PFA (10), GAA (10)	PFA (1.00 ± 0.34), GAA (23903.08 ± 8088.47)	Unpaired t-test	t = 2.955, df = 18 (Two-tailed)	PFA GAA	**	*P* = 0.0085
	Nrxn1α	PFA (10), GAA (10)	PFA (1.00 ± 0.10), GAA (148.59 ± 47.07)	Unpaired t-test	t = 3.136, df = 18 (Two-tailed)	PFA GAA	**	*P* = 0.0057
	NL2	PFA (10), GAA (10)	PFA (1.00 ± 0.11), GAA (63.69 ± 20.22)	Unpaired t-test	t = 3.101, df = 18 (Two-tailed)	PFA GAA	**	*P* = 0.0062
	NL3	PFA (10), GAA (10)	PFA (1.00 ± 0.35), GAA (313.79 ± 102.56)	Unpaired t-test	t = 3.050, df = 18 (Two-tailed)	PFA GAA	**	*P* = 0.0069
Fig. S16	somatostatin	PFA (10), GAA (10)	PFA (1.00 ± 0.04), GAA (0.35 ± 0.07)	Unpaired t-test	t = 7.926, df = 18 (Two-tailed)	PFA GAA	****	P_{adj} < 0.0001
	VIP	PFA (10), GAA (10)	PFA (1.00 ± 0.06), GAA (1.12 ± 0.12)	Unpaired t-test	t = 0.8594, df = 18 (Two-tailed)	PFA GAA	n.s.	*P* = 0.4014
Fig. S17	calbindin	PFA (10), GAA (10)	PFA (1.00 ± 0.03), GAA (1.28 ± 0.12)	Unpaired t-test	t = 2.235, df = 18 (Two-tailed)	PFA GAA	*	*P* = 0.0383
	calretinin	PFA (10), GAA (10)	PFA (1.00 ± 0.05), GAA (7.25 ± 1.70)	Unpaired t-test	t = 3.674, df = 18 (Two-tailed)	PFA GAA	**	*P* = 0.0017
	parvalbumin	PFA (10), GAA (10)	PFA (1.00 ± 0.04), GAA (0.80 ± 0.12)	Unpaired t-test	t = 1.632, df = 18 (Two-tailed)	PFA GAA	n.s.	*P* = 0.1201
Fig. S18	Iba1	PFA (10), GAA (10)	PFA (1.00 ± 0.05), GAA (3.16 ± 0.08)	Unpaired t-test	t = 24.07, df = 18 (Two-tailed)	PFA GAA	****	P_{adj} < 0.0001
	GFAP	PFA (10), GAA (10)	PFA (1.00 ± 0.20), GAA (2.24 ± 0.06)	Unpaired t-test	t = 6.025, df = 18 (Two-tailed)	PFA GAA	****	P_{adj} < 0.0001
	CNPase	PFA (10), GAA (10)	PFA (1.00 ± 0.08), GAA (9.10 ± 0.22)	Unpaired t-test	t = 34.64, df = 18 (Two-tailed)	PFA GAA	****	P_{adj} < 0.0001

Table S3. Summary of improving effects by GAA fixation compared with PFA fixation.

Ionotropic receptors	GA/PFA	Plasmalemmal transporters	GA/PFA
GluA2	**		
GluA3	**	GLAST	****
GluK2	**	GAT1	****
GluN1	****	GlyT2	****
GluN2B	***	CHT	**
GluN2C	****	DAT	***
GluD1	****	NET	****
GluD2	****	HTT	***
$GABA_AR\alpha1$	**	Synaptic vesicle-associated or active zone proteins	GA/PFA
$GABA_AR\gamma2$	**		
Voltage-gated ion channels	**GA/PFA**	Bassoon	**
Nav1.1-1.9 (pan-Nav1.x)	**	CAST	**
Kv1.1	****	synapsin-1	n.s.
Cav2.1	**	**Synaptic adhesion molecules**	**GA/PFA**
Ion channel/receptor-associated proteins	GA/PFA	Cbln1	****
		Cbln3	**
TARP-γ2	**	Nrxn1α	**
TARP-γ8	****	Neuroligin1 (NL1)	****
Shank2	****	Neuroligin2 (NL2)	**
Homer-1	****	Neuroligin3 (NL3)	**
gephyrin	****	**Neuropeptides**	**GA/PFA**
ankyrin-G	****	somatostatin	**** (reduced)
PSD-95	****	VIP	n.s.
SAP-102	****	Cytosolic Ca^{2+}-binding proteins	GA/PFA
Metabotropic receptors and related signaling molecules	GA/PFA		
		calbindin	*
mGluR1	n.s.	calretinin	**
$GABA_BR2$	**	parvalbumin	n.s.
mAChR1	n.s.	**Glial marker proteins**	**GA/PFA**
D1R	****	Iba1	****
IP_3R1	****	GFAP	****
PLCβ1	****	CNPase	****
Vesicular transporters	**GA/PFA**		
VGluT1	**		
VGluT2	****		
VGluT3	***		
VIAAT	**		

VAChT	***		
VMAT2	****		

REFERENCES AND NOTES

1. K. Konno, M. Watanabe, Immunohistochemistry for ion channels and their interacting molecules: Tips for improving antibody accessibility, in *Receptor and Ion Channel Detection in the Brain. Methods and Protocols* (Neuromethods, Springer, 2016), vol. 110, pp. 171–178.

2. A. Lorincz, Z. Nusser, Cell-type-dependent molecular composition of the axon initial segment. *J. Neurosci.* **28**, 14329–14340 (2008).

3. A. Baude, E. Molnár, D. Latawiec, R. A. McIlhinney, P. Somogyi, Synaptic and nonsynaptic localization of the GluR1 subunit of the AMPA-type excitatory amino acid receptor in the rat cerebellum. *J. Neurosci.* **14**, 2830–2843 (1994).

4. A. Baude, Z. Nusser, E. Molnár, R. A. McIlhinney, P. Somogyi, High-resolution immunogold localization of AMPA type glutamate receptor subunits at synaptic and non-synaptic sites in rat hippocampus. *Neuroscience* **69**, 1031–1055 (1995).

5. M. Watanabe, M. Fukaya, K. Sakimura, T. Manabe, M. Mishina, Y. Inoue, Selective scarcity of NMDA receptor channel subunits in the stratum lucidum (mossy fibre-recipient layer) of the mouse hippocampal CA3 subfield. *Eur. J. Neurosci.* **10**, 478–487 (1998).

6. J. M. Fritschy, O. Weinmann, A. Wenzel, D. Benke, Synapse-specific localization of NMDA and $GABA_A$ receptor subunits revealed by antigen-retrieval immunohistochemistry. *J. Comp. Neurol.* **390**, 194–210 (1998).

7. A. Lorincz, Z. Nusser, Molecular identity of dendritic voltage-gated sodium channels. *Science* **328**, 906–909 (2010).

8. M. Fukaya, M. Watanabe, Improved immunohistochemical detection of postsynaptically located PSD-95/SAP90 protein family by protease section pretreatment: A study in the adult mouse brain. *J. Comp. Neurol.* **426**, 572–586 (2000).

9. G. K. McMaster, G. G. Carmichael, Analysis of single- and double-stranded nucleic acids on polyacrylamide and agarose gels by using glyoxal and acridine orange. *Proc. Natl. Acad. Sci. U.S.A.* **74**, 4835–4838 (1977).

10. D. D. Sabatini, K. Bensch, R. J. Barrnett, Cytochemistry and electron microscopy. The preservation of cellular ultrastructure and enzymatic activity by aldehyde fixation. *J. Cell Biol.* **17**, 19–58 (1963).

11. K. N. Richter, N. H. Revelo, K. J. Seitz, M. S. Helm, D. Sarkar, R. S. Saleeb, E. D'Este, J. Eberle, E. Wagner, C. Vogl, D. F. Lazaro, F. Richter, J. Coy-Vergara, G. Coceano, E. S. Boyden, R. R. Duncan, S. W. Hell, M. A. Lauterbach, S. E. Lehnart, T. Moser, T. F. Outeiro, P. Rehling, B. Schwappach, I. Testa, B. Zapiec, S. O. Rizzoli, Glyoxal as an alternative fixative to formaldehyde in immunostaining and super-resolution microscopy. *EMBO J.* **37**, 139–159 (2018).

12. T. Miyazaki, M. Fukaya, H. Shimizu, M. Watanabe, Subtype switching of vesicular glutamate transporters at parallel fibre-Purkinje cell synapses in developing mouse cerebellum. *Eur. J. Neurosci.* **17**, 2563–2572 (2003).

13. M. Uchigashima, T. Ohtsuka, K. Kobayashi, M. Watanabe, Dopamine synapse is a neuroligin-2-mediated contact between dopaminergic presynaptic and GABAergic postsynaptic structures. *Proc. Natl. Acad. Sci. U.S.A.* **113**, 4206–4211 (2016).

14. A. S. Landsend, M. Amiry-Moghaddam, A. Matsubara, L. Bergersen, S. Usami, R. J. Wenthold, O. P. Ottersen, Differential localization of delta glutamate receptors in the rat cerebellum: Coexpression with AMPA receptors in parallel fiber-spine synapses and absence from climbing fiber-spine synapses. *J. Neurosci.* **17**, 834–842 (1997).

15. K. Konno, K. Matsuda, C. Nakamoto, M. Uchigashima, T. Miyazaki, M. Yamasaki, K. Sakimura, M. Yuzaki, M. Watanabe, Enriched expression of GluD1 in higher brain regions and its involvement in parallel fiber-interneuron synapse formation in the cerebellum. *J. Neurosci.* **34**, 7412–7424 (2014).

16. C. Nakamoto, K. Konno, T. Miyazaki, E. Nakatsukasa, R. Natsume, M. Abe, M. Kawamura, Y. Fukazawa, R. Shigemoto, M. Yamasaki, K. Sakimura, M. Watanabe, Expression mapping,

quantification, and complex formation of GluD1 and GluD2 glutamate receptors in adult mouse brain. *J. Comp. Neurol.* **528**, 1003–1027 (2020).

17. M. Watanabe, Y. Inoue, K. Sakimura, M. Mishina, Developmental changes in distribution of NMDA receptor channel subunit mRNAs. *Neuroreport* **3**, 1138–1140 (1992).

18. M. Watanabe, Y. Inoue, K. Sakimura, M. Mishina, Distinct distributions of five N-methyl-D-aspartate receptor channel subunit mRNAs in the forebrain. *J. Comp. Neurol.* **338**, 377–390 (1993).

19. M. Abe, M. Fukaya, T. Yagi, M. Mishina, M. Watanabe, K. Sakimura, NMDA receptor GluRepsilon/NR2 subunits are essential for postsynaptic localization and protein stability of GluRzeta1/NR1 subunit. *J. Neurosci.* **24**, 7292–7304 (2004).

20. K. Akashi, T. Kakizaki, H. Kamiya, M. Fukaya, M. Yamasaki, M. Abe, R. Natsume, M. Watanabe, K. Sakimura, NMDA receptor GluN2B (GluR epsilon 2/NR2B) subunit is crucial for channel function, postsynaptic macromolecular organization, and actin cytoskeleton at hippocampal CA3 synapses. *J. Neurosci.* **29**, 10869–10882 (2009).

21. K. Yamada, M. Fukaya, H. Shimizu, K. Sakimura, M. Watanabe, NMDA receptor subunits GluRepsilon1, GluRepsilon3 and GluRzeta1 are enriched at the mossy fibre-granule cell synapse in the adult mouse cerebellum. *Eur. J. Neurosci.* **13**, 2025–2036 (2001).

22. J. G. Valtschanoff, A. Burette, R. J. Wenthold, R. J. Weinberg, Expression of NR2 receptor subunit in rat somatic sensory cortex: Synaptic distribution and colocalization with NR1 and PSD-95. *J. Comp. Neurol.* **410**, 599–611 (1999).

23. M. Yamasaki, M. Fukaya, M. Yamazaki, H. Azechi, R. Natsume, M. Abe, K. Sakimura, M. Watanabe, TARP γ-2 and γ-8 differentially control AMPAR density across schaffer collateral/commissural synapses in the hippocampal CA1 area. *J. Neurosci.* **36**, 4296–4312 (2016).

24. T. Takeuchi, T. Miyazaki, M. Watanabe, H. Mori, K. Sakimura, M. Mishina, Control of synaptic connection by glutamate receptor delta2 in the adult cerebellum. *J. Neurosci.* **25**, 2146–2156 (2005).

25. A. Iwakura, M. Uchigashima, T. Miyazaki, M. Yamasaki, M. Watanabe, Lack of molecular-anatomical evidence for GABAergic influence on axon initial segment of cerebellar Purkinje cells by the pinceau formation. *J. Neurosci.* **32**, 9438–9448 (2012).

26. M. Yamazaki, M. Fukaya, K. Hashimoto, M. Yamasaki, M. Tsujita, M. Itakura, M. Abe, R. Natsume, M. Takahashi, M. Kano, K. Sakimura, M. Watanabe, TARPs gamma-2 and gamma-7 are essential for AMPA receptor expression in the cerebellum. *Eur. J. Neurosci.* **31**, 2204–2220 (2010).

27. T. Miyazaki, M. Yamasaki, K. Hashimoto, M. Yamazaki, M. Abe, H. Usui, M. Kano, K. Sakimura, M. Watanabe, $Ca_V2.1$ in cerebellar Purkinje cells regulates competitive excitatory synaptic wiring, cell survival, and cerebellar biochemical compartmentalization. *J. Neurosci.* **32**, 1311–1328 (2012).

28. K. Ichtchenko, Y. Hata, T. Nguyen, B. Ullrich, M. Missler, C. Moomaw, T. C. Südhof, Neuroligin 1: A splice site-specific ligand for beta-neurexins. *Cell* **81**, 435–443 (1995).

29. M. Yamasaki, T. Miyazaki, H. Azechi, M. Abe, R. Natsume, T. Hagiwara, A. Aiba, M. Mishina, K. Sakimura, M. Watanabe, Glutamate receptor δ2 is essential for input pathway-dependent regulation of synaptic AMPAR contents in cerebellar Purkinje cells. *J. Neurosci.* **31**, 3362–3374 (2011).

30. M. Watanabe, Production of high-quality antibodies for the study of receptors and ion channels, in *Receptor and Ion Channel Detection in the Brain. Methods and Protocols* (Neuromethods, Springer, 2016), vol. 110, pp. 3–18.

31. E. Miura, M. Fukaya, T. Sato, K. Sugihara, M. Asano, K. Yoshioka, M. Watanabe, Expression and distribution of JNK/SAPK-associated scaffold protein JSAP1 in developing and adult mouse brain. *J. Neurochem.* **97**, 1431–1446 (2006).

32. T. Miyazaki, M. Yamasaki, K. F. Tanaka, M. Watanabe, Compartmentalized input-output organization of lugaro cells in the cerebellar cortex. *Neuroscience* **462**, 89–105 (2021).

33. E. Miura, K. Matsuda, J. I. Morgan, M. Yuzaki, M. Watanabe, Cbln1 accumulates and colocalizes with Cbln3 and GluRdelta2 at parallel fiber-Purkinje cell synapses in the mouse cerebellum. *Eur. J. Neurosci.* **29**, 693–706 (2009).

34. T. Iijima, E. Miura, K. Matsuda, Y. Kamekawa, M. Watanabe, M. Yuzaki, Characterization of a transneuronal cytokine family Cbln - regulation of secretion by heteromeric assembly. *Eur. J. Neurosci.* **25**, 1049–1057 (2007).

35. M. Narushima, M. Uchigashima, K. Hashimoto, M. Watanabe, M. Kano, Depolarization-induced suppression of inhibition mediated by endocannabinoids at synapses from fast-spiking interneurons to medium spiny neurons in the striatum. *Eur. J. Neurosci.* **24**, 2246–2252 (2006).

36. M. Uchigashima, M. Narushima, M. Fukaya, I. Katona, M. Kano, M. Watanabe, Subcellular arrangement of molecules for 2-arachidonoyl-glycerol-mediated retrograde signaling and its physiological contribution to synaptic modulation in the striatum. *J. Neurosci.* **27**, 3663–3676 (2007).

37. R. Ichikawa, M. Yamasaki, T. Miyazaki, K. Konno, K. Hashimoto, H. Tatsumi, Y. Inoue, M. Kano, M. Watanabe, Developmental switching of perisomatic innervation from climbing fibers to basket cell fibers in cerebellar Purkinje cells. *J. Neurosci.* **31**, 16916–16927 (2011).

38. K. Hisano, M. Watanabe, Y. Morimoto, Protective effects of the free radical scavenger edaravone against glutamate neurotoxicity in nearly pure neuronal culture. *J. Anesth.* **23**, 363–369 (2009).

39. T. Shibata, K. Yamada, M. Watanabe, K. Ikenaka, K. Wada, K. Tanaka, Y. Inoue, Glutamate transporter GLAST is expressed in the radial glia-astrocyte lineage of developing mouse spinal cord. *J. Neurosci.* **17**, 9212–9219 (1997).

40. M. Fukaya, M. Tsujita, M. Yamazaki, E. Kushiya, M. Abe, K. Akashi, R. Natsume, M. Kano, H. Kamiya, M. Watanabe, K. Sakimura, Abundant distribution of TARP γ-8 in synaptic and extrasynaptic surface of hippocampal neurons and its major role in AMPA receptor expression on spines and dendrites. *Eur. J. Neurosci.* **24**, 2177–2190 (2006).

41. G. G. Nagy, M. Al-Ayyan, D. Andrew, M. Fukaya, M. Watanabe, A. J. Todd, Widespread expression of the AMPA receptor GluR2 subunit at glutamatergic synapses in the rat spinal cord and phosphorylation of GluR1 in response to noxious stimulation revealed with an antigen-unmasking method. *J. Neurosci.* **24**, 5766–5777 (2004).

42. D. Yan, M. Yamasaki, C. Straub, M. Watanabe, S. Tomita, Homeostatic control of synaptic transmission by distinct glutamate receptors. *Neuron* **78**, 687–699 (2013).

43. M. Hondo, N. Furutani, M. Yamasaki, M. Watanabe, T. Sakurai, Orexin neurons receive glycinergic innervations. *PLOS ONE* **6**, e25076 (2011).

44. M. Nakamura, K. Sato, M. Fukaya, K. Araishi, A. Aiba, M. Kano, M. Watanabe, Signaling complex formation of phospholipase Cbeta4 with metabotropic glutamate receptor type 1alpha and 1,4,5-trisphosphate receptor at the perisynapse and endoplasmic reticulum in the mouse brain. *Eur. J. Neurosci.* **20**, 2929–2944 (2004).

45. J. Somogyi, A. Baude, Y. Omori, H. Shimizu, S. El Mestikawy, M. Fukaya, R. Shigemoto, M. Watanabe, P. Somogyi, GABAergic basket cells expressing cholecystokinin contain vesicular glutamate transporter type 3 (VGLUT3) in their synaptic terminals in hippocampus and isocortex of the rat. *Eur. J. Neurosci.* **19**, 552–569 (2004).

46. M. Narushima, M. Uchigashima, M. Fukaya, M. Matsui, T. Manabe, K. Hashimoto, M. Watanabe, M. Kano, Tonic enhancement of endocannabinoid-mediated retrograde suppression of inhibition by cholinergic interneuron activity in the striatum. *J. Neurosci.* **27**, 496–506 (2007).

47. J. Tanaka, S. Nakagawa, E. Kushiya, M. Yamasaki, M. Fukaya, T. Iwanaga, M. I. Simon, K. Sakimura, M. Kano, M. Watanabe, Gq protein alpha subunits Galphaq and Galpha11 are localized at postsynaptic extra-junctional membrane of cerebellar Purkinje cells and hippocampal pyramidal cells. *Eur. J. Neurosci.* **12**, 781–792 (2000).

48. M. Fukaya, M. Uchigashima, S. Nomura, Y. Hasegawa, H. Kikuchi, M. Watanabe, Predominant expression of phospholipase Cbeta1 in telencephalic principal neurons and cerebellar interneurons, and its close association with related signaling molecules in somatodendritic neuronal elements. *Eur. J. Neurosci.* **28**, 1744–1759 (2008).

49. K. Matsuda, E. Miura, T. Miyazaki, W. Kakegawa, K. Emi, S. Narumi, Y. Fukazawa, A. Ito-Ishida, T. Kondo, R. Shigemoto, M. Watanabe, M. Yuzaki, Cbln1 is a ligand for an orphan glutamate receptor delta2, a bidirectional synapse organizer. *Science* **328**, 363–368 (2010).

50. Y. Kawamura, M. Fukaya, T. Maejima, T. Yoshida, E. Miura, M. Watanabe, T. Ohno-Shosaku, M. Kano, The CB1 cannabinoid receptor is the major cannabinoid receptor at excitatory presynaptic sites in the hippocampus and cerebellum. *J. Neurosci.* **26**, 2991–3001 (2006).